Published for SISSA by Springer

Received: May 1, 2024
Accepted: June 12, 2024
Published: July 9, 2024

Two-loop integrals for $t\bar{t}$+jet production at hadron colliders in the leading colour approximation

Simon Badger,[a] **Matteo Becchetti**,[b] **Nicolò Giraudo**[c] **and Simone Zoia**[d]

[a] *Physics Department, Torino University and INFN Torino, Via Pietro Giuria 1, I-10125 Torino, Italy*
[b] *Dipartimento di Fisica e Astronomia, Università di Bologna e INFN, Sezione di Bologna, via Irnerio 46, I-40126 Bologna, Italy*
[c] *Physik-Institut, Universität Zürich, Winterthurerstrasse 190, CH-8057 Zürich, Switzerland*
[d] *CERN, Theoretical Physics Department, CH-1211 Geneva 23, Switzerland*

E-mail: simondavid.badger@unito.it, matteo.becchetti@unibo.it, nicolo.giraudo@physik.uzh.ch, simone.zoia@cern.ch

Abstract: We compute the differential equations for the two remaining integral topologies contributing to the leading colour two-loop amplitudes for $pp \to t\bar{t}j$. We derive differential equations for the master integrals by solving the integration-by-parts identities over finite fields. Of the two systems of differential equations, one is presented in canonical 'd log' form, while the other is found to have an elliptic sector. For the elliptic topology we identify the relevant elliptic curve, and present the differential equations in a more general form which depends quadratically on ε and contains non-logarithmic one-forms in addition to the canonical d log's. We solve the systems of differential equations numerically using generalised series expansions with the boundary terms obtained using the auxiliary mass flow method. A summary of all one-loop and two-loop planar topologies is presented including the list of alphabet letters for the 'd log' form systems and high-precision boundary values.

Keywords: Higher-Order Perturbative Calculations, Top Quark

ArXiv ePrint: 2404.12325

https://doi.org/10.1007/JHEP07(2024)073

JHEP07(2024)073

Contents

JHEP07(2024)073

1 Introduction

Precision tests of the Standard Model (SM) in the top quark sector are essential part of the current physics program at high energy colliders. Observables involving a top-quark pair have a wide variety of applications, and can be used to constrain SM parameters and parton distribution functions. Furthermore, they are also important backgrounds for other searches. Top-quark pair production in association with at least one hard jet forms a significant fraction, around 50%, of all top-quark pair events and has been studied extensively by both ATLAS and CMS experiments [1–4].

The normalised differential cross section for the $t\bar{t}j$ invariant mass in top-quark pair production in association with one jet ($pp \to t\bar{t}j$) has been proposed as an observable highly sensitive to the top-quark mass [5]. Phenomenological studies and experimental analyses at next-to-leading order (NLO) in QCD have already demonstrated this as a viable method for the extraction of the mass with current experimental data [6–8]. While the

current experimental and theoretical uncertainties are comparable, higher order theoretical predictions will be necessary to make significant improvements as more data become available.

Precision theoretical predictions for top-quark processes present one of the most challenging classes of computation. The presence of internal massive particles creates analytic complexity in the corresponding Feynman integrals, which means that conventional methods for their numerical evaluation can fail. How to achieve a fast and stable evaluation of the integrals remains an active field of research, see [9] and references therein. Coupling this with the multiple scales associated with the three-parton final states makes processes such as $pp \to t\bar{t}j$ and $pp \to t\bar{t}W/Z/H$ seriously daunting computations.

The NLO QCD corrections have been available since 2007 [10, 11]. Remarkable theoretical developments since then now enable a broad range of phenomenological predictions including full off-shell decays and interfaces with parton shower [12–16], as well as mixed QCD and EW corrections [17]. Improving on the theoretical precision requires going to next-to-next-to-leading order (NNLO) in QCD and, while the tree-level and one-loop level amplitude ingredients can be provided by the current generation of automated tools [18], the two-loop amplitudes remain a bottleneck. In this article, we continue the task of computing the two-loop QCD corrections to top-quark pair production in association with a jet that was initiated in refs. [19, 20]. The preliminary tasks undertaken so far explored the kinematic complexity of the helicity amplitudes at one-loop up to $\mathcal{O}(\varepsilon^2)$ in the dimensional regularisation parameter ε, and the computation of master integrals relevant for a single 'pentagon-box' two-loop integral family via canonical form differential equations [21–23].

The last few years have seen rapid progress for $2 \to 3$ scattering amplitudes with massless internal propagators, in which a lot has been understood for both the relevant Feynman integrals and the analytic representation of the amplitudes. Two new methods have had a major impact on these developments: the widespread use of finite field modular arithmetic for algebraic manipulations and rational function reconstruction [24–26], and the construction of special function bases, commonly referred to as 'pentagon functions', suitable for fast and stable numerical evaluations [27–31]. Thanks to these developments, a plethora of new results have now been obtained for the one- and two-loop five-particle Feynman integrals relevant for the cases with no or one external massive particle [27, 31–37], scattering amplitudes [27, 33, 38–63], and differential distributions at NNLO QCD accuracy [58, 61, 64–71]. The first results for massless six-particle kinematics have also recently appeared [72, 73] together with the first steps investigating processes involving internal massive propagators [19, 20, 74–76]. Approximations of the two-loop amplitudes for $pp \to t\bar{t}H$ may also be used to make precise phenomenological predictions [77, 78].

This article presents the completion of the Feynman integral topologies needed for $pp \to t\bar{t}j$ at two loops in the leading colour approximation. The construction of the master integral bases and their evaluation follow the methodology used in the previous works [19, 20]. Of the two new pentagon-box topologies that appear, one is shown to have some complicated features that go against the conventional wisdom for what should appear for a leading colour, planar configuration. In particular, we find that one sector requires the use of a nested square root in order to rotate the differential equations into an ε-factorised form (see section 3.3). This feature is perhaps not completely unexpected since it has been observed before albeit

JHEP07(2024)073

with more complicated kinematics such as $pp \to t\bar{t}H$ [74]. The second feature is that one sector contains elliptic integrals (see section 3.5). This is perhaps more surprising, as no sub-sectors of this topology were previously known to be elliptic, although there are no principles forbidding it. Both of these features mean that the route towards a well defined basis of special functions which can be efficiently evaluated numerically is unclear. Canonical form differential equations have been studied in the case of elliptic Feynman integrals although not for such complicated kinematics [79–84]. Therefore in this article we present a compact representation of the differential equations, which are not ε-factorised, in terms of a minimal set of independent one-forms, and show that they can be reliably solved through generalised series expansions [85].

The computation of the differential equations satisfied by the integral bases requires the solution of systems of Integration-by-Parts (IBPs) identities [86, 87], which we generate using LiteRed [88, 89] and NeatIBP [90]. The latter package, in particular, allows us to obtain optimised systems of IBP relations through the solution of syzygy equations [91], this way making their solution substantially simpler. We solve the IBP relations with the Laporta algorithm [92] within the FiniteFlow framework [26, 93].

While we do not obtain canonical differential equations for the family involving elliptic integrals, we do put some effort into making their analytic properties transparent. In particular, we identify the elliptic curve associated with the appearing elliptic integrals. Furthermore, we express the differential equations in terms of a set of linearly independent one-forms. We arrange the latter to be logarithmic as much as possible, in analogy with the usual canonical differential equations. Only the one-forms which relate master integrals involving either the elliptic curve or the nested square root are non-logarithmic. This makes the expression of the differential equations compact, and separates out clearly the features in common with the standard canonical cases from the more complicated ones. We expect that this information will be precious in view of future work to obtain a canonical form for the differential equations of this topology as well.

We provide a semi-analytic solution to the differential equations for the master integrals by means of the multivariate generalisation of the method of generalised power series expansions [94–100] proposed in ref. [85] and implemented in a number of public Mathematica packages [101–103]. In particular, we make use of DiffExp [101]. The solution to the differential equations is fully characterised once a set of boundary values is given. We obtain high-precision numerical boundary values by using the Mathematica package AMFlow [102], which implements the auxiliary mass flow method [104–106]. We use the interface to FiniteFlow [26] and LiteRed [88, 89] for the required IBP reduction.

The paper is structured as follows. In section 2 we define the pentagon-box topologies under study and describe the computational framework. In section 3 we discuss the construction and the analytic features of the master integral bases. Section 4 is devoted to the one-form representation of the differential equations, while in section 5 we discuss the numerical evaluation of the master integrals. We draw our conclusions and give an outlook on future developments in section 6. Finally, we identify the elliptic curve underlying the analytic structure of the Feynman integrals in the elliptic sector in appendix A, define the one-loop families in appendix B, and describe the supplementary material in appendix C.

JHEP07(2024)073

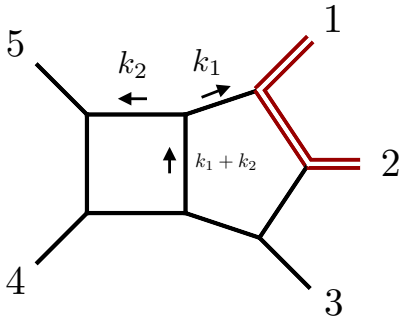

(a) Topology PB_A.

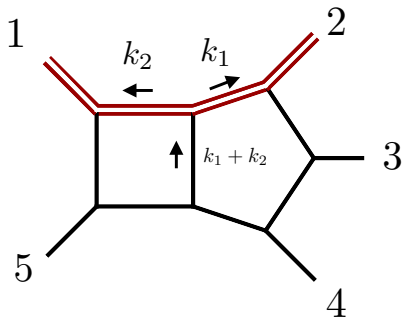

(b) Topology PB_B.

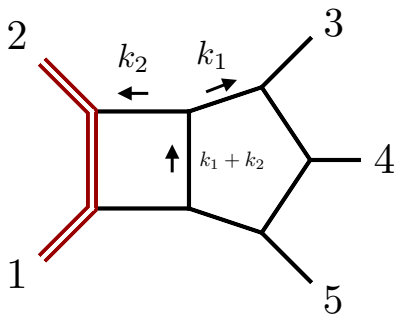

(c) Topology PB_C.

Figure 1. The three pentagon-box topologies contributing to $pp \to t\bar{t}j$ in the leading colour limit. Black lines denote massless particles and red double-lines denote massive particles.

2 Notation and definitions

In this article we consider the three two-loop pentagon-box integral topologies shown in figure 1. In addition, we present an explicitly 'd log' form for all one-loop pentagon integrals, which we define in appendix B. The integrals of the pentagon-box topology $F \in \{\mathrm{PB}_A, \mathrm{PB}_B, \mathrm{PB}_C\}$ have the form

$$I^{(F),a_9,a_{10},a_{11}}_{a_1,a_2,a_3,a_4,a_5,a_6,a_7,a_8} = \int \mathcal{D}^d k_1 \, \mathcal{D}^d k_2 \, \frac{D_{F,9}^{a_9} D_{F,10}^{a_{10}} D_{F,11}^{a_{11}}}{D_{F,1}^{a_1} \cdots D_{F,8}^{a_8}} \,, \tag{2.1}$$

where $a_1, \cdots, a_{11} \geq 0$ and $d = 4 - 2\varepsilon$. The integration measure is

$$\mathcal{D}^d k_i = \mathrm{e}^{\varepsilon \gamma_{\mathrm{E}}} \frac{\mathrm{d}^d k_i}{\mathrm{i}\pi^{\frac{d}{2}}} \,. \tag{2.2}$$

The inverse propagators $D_{F,i}$ are defined in table 1. Note that $D_{F,9}$, $D_{F,10}$ and $D_{F,11}$ are irreducible scalar products.

The external momenta p_i are considered as outgoing from the graphs and all the particles are on-shell, i.e. $p_1^2 = p_2^2 = m_t^2$ while $p_3^2 = p_4^2 = p_5^2 = 0$. The kinematics of the integrals can be described in terms of six independent Lorentz invariants. Here we choose the top-quark mass m_t^2 and the five adjacent scalar products,

$$\vec{x} = \{d_{12}, d_{23}, d_{34}, d_{45}, d_{15}, m_t^2\} \,, \tag{2.3}$$

JHEP07(2024)073

	PB_A	PB_B	PB_C
$D_{F,1}$	k_1^2	$k_1^2 - m_t^2$	k_1^2
$D_{F,2}$	$(k_1 - p_1)^2 - m_t^2$	$(k_1 - p_2)^2$	$(k_1 - p_3)^2$
$D_{F,3}$	$(k_1 - p_1 - p_2)^2$	$(k_1 - p_2 - p_3)^2$	$(k_1 - p_3 - p_4)^2$
$D_{F,4}$	$(k_1 - p_1 - p_2 - p_3)^2$	$(k_1 - p_2 - p_3 - p_4)^2$	$(k_1 - p_3 - p_4 - p_5)^2$
$D_{F,5}$	k_2^2	$k_2^2 - m_t^2$	k_2^2
$D_{F,6}$	$(k_2 - p_5)^2$	$(k_2 - p_1)^2$	$(k_2 - p_2)^2 - m_t^2$
$D_{F,7}$	$(k_2 - p_4 - p_5)^2$	$(k_2 - p_1 - p_5)^2$	$(k_2 - p_1 - p_2)^2$
$D_{F,8}$	$(k_1 + k_2)^2$	$(k_1 + k_2)^2$	$(k_1 + k_2)^2$
$D_{F,9}$	$(k_1 + p_5)^2$	$(k_1 + p_1)^2 - m_t^2$	$(k_1 + p_2)^2 - m_t^2$
$D_{F,10}$	$(k_2 + p_1)^2 - m_t^2$	$(k_2 + p_2)^2 - m_t^2$	$(k_2 + p_3)^2$
$D_{F,11}$	$(k_2 + p_1 + p_2)^2$	$(k_2 + p_2 + p_3)^2 - m_t^2$	$(k_2 + p_3 + p_4)^2$

Table 1. Inverse propagators $D_{F,i}$ of the pentagon-box topologies shown in figure 1.

where

$$d_{ij} = p_i \cdot p_j \,. \tag{2.4}$$

The minimal set of master integrals (MIs) is obtained by IBP reduction as discussed in the introduction. Topology PB_A has been considered previously in ref. [20] and has 88 MIs. For the new cases presented here we find 121 MIs for topology PB_B and 109 for topology PB_C.[1]

We find a set of 14 square roots appearing in the differential equations and associated alphabet for all one-loop and planar two-loop topologies. These are defined as

$$\beta_{12} = \sqrt{\frac{\det G(p_1,p_2)}{s_{12}}} = \sqrt{1 - \frac{4m_t^2}{s_{12}}}\,, \tag{2.5}$$

$$\beta_{34} = \sqrt{1 - \frac{4m_t^2}{s_{34}}}\,, \tag{2.6}$$

$$\beta_{45} = \sqrt{1 - \frac{4m_t^2}{s_{45}}}\,, \tag{2.7}$$

$$\Delta_{3,1} = \sqrt{-\det G(p_1,p_{23})}\,, \tag{2.8}$$

$$\Delta_{3,2} = \sqrt{-\det G(p_2,p_{15})}\,, \tag{2.9}$$

$$\Delta_{3,3} = \sqrt{-\det G(p_1,p_{25})}\,, \tag{2.10}$$

$$\Delta_{3,4} = \sqrt{-\det G(p_2,p_{13})}\,, \tag{2.11}$$

$$\Lambda_1 = \sqrt{\frac{\det Y^{0mm0}_{p_1|p_3|p_2|p_{45}}}{d_{23}^2 d_{13}^2}}\,, \tag{2.12}$$

$$\Lambda_2 = \sqrt{\frac{\det Y^{0mmm}_{p_2|p_3|p_4|p_{51}}}{d_{23}^2 d_{34}^2}}\,, \tag{2.13}$$

$$\Lambda_3 = \sqrt{\frac{\det Y^{m0mm}_{p_{13}|p_2|p_4|p_5}}{d_{24}^2 d_{45}^2}}\,, \tag{2.14}$$

$$\Lambda_4 = \sqrt{\frac{\det Y^{m0mm}_{p_1|p_{23}|p_4|p_5}}{d_{15}^2 d_{45}^2}}\,, \tag{2.15}$$

$$\Lambda_5 = \sqrt{\frac{\det Y^{mmmm}_{p_{12}|p_3|p_4|p_5}}{d_{34}^2 d_{45}^2}}\,, \tag{2.16}$$

$$\Lambda_6 = \sqrt{(s_{15} - s_{23})^2 + \frac{4 s_{34} s_{45} m_t^2}{s_{12}}}\,, \tag{2.17}$$

$$\mathrm{tr}_5 = 4\sqrt{\det G(p_3,p_4,p_5,p_1)}\,, \tag{2.18}$$

[1] NeatIBP finds additional symmetry relations with respect to LiteRed, reducing the number of MIs by 2 for each topology PB_B and PB_C. The missing relations are a result of both particles 1 and 2 having the same mass.

JHEP07(2024)073

where $G_{ij}(\vec{v}) = v_i \cdot v_j$ is the Gram matrix, $p_{ij} = p_i + p_j$, $s_{ij} = (p_i + p_j)^2$, and m denotes m_t for the sake of compactness. $Y^{m_1 \ldots m_4}_{P_1|\ldots|P_4}$ represents the Cayley matrices associated with one-loop box configurations appearing at sub-leading colour, which are defined by

$$\left[Y^{m_1 m_2 m_3 m_4}_{P_1|P_2|P_3|P_4}\right]_{ij} = \frac{1}{2}\left[(q_i - q_j)^2 - m_i^2 - m_j^2\right], \qquad q_i = \sum_{k=0}^{i-1} P_k\,, \tag{2.19}$$

for $i, j = 1, \ldots, 4$, with $P_0 = 0$. Λ_6 only appears at two loops.

Note that tr_5 is related to the five-point pseudo-scalar invariant via

$$\mathrm{tr}_5^2 = \mathrm{tr}(\gamma_5 \not{p}_3 \not{p}_4 \not{p}_5 \not{p}_1)^2\,. \tag{2.20}$$

We refrain from identifying tr_5 with $\mathrm{tr}(\gamma_5 \not{p}_3 \not{p}_4 \not{p}_5 \not{p}_1)$, as the latter is a parity-odd object, i.e. it changes sign under space-time parity conjugation and odd-signature permutations. The parity degree of freedom is required to describe scattering amplitudes, but not for the computation of Feynman integrals. We therefore prefer to define tr_5 as the parity-even square root in eq. (2.18). Furthermore, we will make use of the short-hand

$$\mathrm{tr}_\pm\left[\not{p}_i \not{p}_j \not{p}_k \not{p}_l\right] = \frac{1}{2}\,\mathrm{tr}\left[\not{p}_i \not{p}_j \not{p}_k \not{p}_l (1 \pm \gamma_5)\right] \tag{2.21}$$

to make certain expressions more compact. We however remove the parity degree of freedom in them by replacing the parity-odd trace $\mathrm{tr}(\gamma_5 \not{p}_3 \not{p}_4 \not{p}_5 \not{p}_1)$ with the parity-even square root tr_5 defined in eq. (2.18).

In order to write compact expressions for the MIs which satisfy canonical differential equations, we use choices motivated by the local numerators introduced in refs. [27, 35, 107–109]. In $d = 4 - 2\varepsilon$ dimensions, we can find numerator insertions that can be written in terms of the -2ε dimensional components of the loop momenta and are conventionally denoted μ_{ij},

$$k_i = k_i^{[4]} + k_i^{[-2\varepsilon]}, \qquad \mu_{ij} = -k_i^{[-2\varepsilon]} \cdot k_j^{[-2\varepsilon]}. \tag{2.22}$$

We denote these numerator insertions using an additional superscript $[ij]$, as

$$\begin{aligned} I^{(F),[ij],a_9,a_{10},a_{11}}_{a_1,a_2,a_3,a_4,a_5,a_6,a_7,a_8} &= \int \mathcal{D}^d k_1\, \mathcal{D}^d k_2\, \mu_{ij}\, \frac{D_{F,9}^{a_9} D_{F,10}^{a_{10}} D_{F,11}^{a_{11}}}{D_{F,1}^{a_1} \cdots D_{F,8}^{a_8}}\,, \\ I^{(F),[ij,kl],a_9,a_{10},a_{11}}_{a_1,a_2,a_3,a_4,a_5,a_6,a_7,a_8} &= \int \mathcal{D}^d k_1\, \mathcal{D}^d k_2\, \mu_{ij}\, \mu_{kl}\, \frac{D_{F,9}^{a_9} D_{F,10}^{a_{10}} D_{F,11}^{a_{11}}}{D_{F,1}^{a_1} \cdots D_{F,8}^{a_8}}\,. \end{aligned} \tag{2.23}$$

3 Master integral bases

In this section we discuss the construction of the bases of master integrals for topology PB_B and PB_C, and describe their features. The guiding principle in this construction is the simplification of the differential equations (DEs) satisfied by the MIs. Let $\vec{\mathcal{I}}_F$ be the list of MIs for topology F. In general, $\vec{\mathcal{I}}_F$ satisfies a system of DEs of the form [21, 110–113]

$$\frac{\partial}{\partial x_i}\vec{\mathcal{I}}_F(\vec{x}, \varepsilon) = A^{(F)}_{x_i}(\vec{x}, \varepsilon) \cdot \vec{\mathcal{I}}_F(\vec{x}, \varepsilon)\,, \tag{3.1}$$

JHEP07(2024)073

for every $i = 1, \ldots, 6$. The matrices $A^{(F)}_{x_i}$ are called *connection matrices*. We rewrite eq. (3.1) in a more compact form by introducing the total differential with respect to the kinematic invariants, d, as

$$\mathrm{d}\,\vec{\mathcal{I}}_F(\vec{x},\varepsilon) = \mathrm{d}A^{(F)}(\vec{x},\varepsilon)\cdot\vec{\mathcal{I}}_F(\vec{x},\varepsilon)\,, \tag{3.2}$$

where $\mathrm{d}A^{(F)}$ is the matrix-valued one-form

$$\mathrm{d}A^{(F)}(\vec{x},\varepsilon) = \sum_{i=1}^{6} A^{(F)}_{x_i}(\vec{x},\varepsilon)\;\mathrm{d}x_i\,. \tag{3.3}$$

With a slight abuse of notation, we refer to $\mathrm{d}A^{(F)}(\vec{x},\varepsilon)$ as connection matrix as well. The solution to eq. (3.2) is enormously simplified if a choice of MIs is found such that the DEs take the *canonical form* [23]

$$\mathrm{d}\,\vec{\mathcal{I}}_F(\vec{x},\varepsilon) = \varepsilon\,\mathrm{d}A^{(F)}(\vec{x})\,\vec{\mathcal{I}}_F(\vec{x},\varepsilon)\,, \tag{3.4}$$

where the dependence of the connection matrices on ε is factorised, and $\mathrm{d}A^{(F)}(\vec{x})$ is a linear combination of logarithmic one-forms:

$$\mathrm{d}A^{(F)}(\vec{x}) = \sum_i c_i^{(F)}\mathrm{d}\log\left(W_i(\vec{x})\right)\,. \tag{3.5}$$

Here, the $c_i^{(F)}$ are matrices of rational numbers, and the *letters* $W_i(\vec{x})$ are algebraic functions of the kinematic invariants $\vec{x}$. Their ensemble, called *alphabet*, dictates the singularity structure of the MIs. The factorisation of ε allows us to express the solution algorithmically in terms of Chen iterated integrals [114], order by order in the Laurent expansion around $\varepsilon = 0$. This, in conjunction with the presence of logarithmic one-forms only, enables the application of a well-established toolbox of mathematical techniques — most notably the symbol [115] — to write down and manipulate the solution. Building on this, the method of the so-called *pentagon functions* [28–31, 54, 74, 116] has proven particularly successful in the computation of two-loop amplitudes for $2 \to 3$ processes.

It is however known that the DEs for Feynman integrals can take more complicated forms. Indeed, we anticipate that the canonical form in eqs. (3.4) and (3.5) can only be achieved for topologies PB_A and PB_C, whereas a generalisation is necessary for topology PB_B. First of all, it is not proven that one can always factorise the dependence on ε in the connection matrices. On top of that, even when ε is factorised, one-forms other than d log's may be necessary (see e.g. the review [9] and references therein). For such cases, the notion of 'canonical' DEs is still under debate [80, 83]. On the one hand, the techniques for bringing the DEs to an ε-factorised form are much less mature than in the d log case. Moreover, even when an ε-factorised form is achieved which involves one-forms more complicated than the d log's in eq. (3.5), manipulating and evaluating the solution efficiently remain challenging. For these reasons, it is often convenient to resort to more flexible numerical approaches to solve DEs beyond the d log case, as opposed to fully analytic solutions in terms of well understood special functions. The method of generalised power series expansions [85] is proving particularly effective, boosted by the availability of public implementations [101–103].

JHEP07(2024)073

Nonetheless, also within this approach to the solution, simplifying as much as possible the form of the DEs is crucial to an efficient and stable evaluation of the solution. In particular, it is desirable for the connection matrices to depend polynomially on ε, and for the degree in ε to be as low as possible. More explicitly, in the generalisation of the canonical DEs we consider in this work for topology PB_B, the connection matrix has the form

$$\mathrm{d}A^{(\mathrm{PB}_B)}(\vec{x},\varepsilon) = \sum_{k=0}^{k_{\max}} \sum_i \varepsilon^k \, c_{k,i}^{(\mathrm{PB}_B)} \, \omega_i(\vec{x}) \,, \tag{3.6}$$

where $\omega_i(\vec{x})$ are (linearly independent) *one-forms*, $k_{\max} \in \mathbb{N}$, and $c_{k,i}^{(\mathrm{PB}_B)}$ are matrices of rational numbers. More explicitly, the one-forms have the form

$$\omega_i(\vec{x}) = \mathcal{C}_i(\vec{x}) \sum_{j=1}^{6} f_{ij}(\vec{x}) \, \mathrm{d}x_j \,, \tag{3.7}$$

where $f_{ij}(\vec{x})$ are rational functions, and $\mathcal{C}_i(\vec{x})$ is either 1 or a square root (possibly a product of square roots). A subset of the one-forms $\{\omega_i(\vec{x})\}$ may be logarithmic, i.e., for some one-form $\omega(\vec{x})$ there may exist $W(\vec{x})$ such that $\omega(\vec{x}) = \mathrm{d}\log W(\vec{x})$. In this case, we recall that $W(\vec{x})$ is called *letter*.

Equation (3.7) implies that each one-form (including the logarithmic ones) possesses a property called *charge* with respect to the square roots of the problem. With respect to each square root $\mathcal{C}$, a one-form ω is either *even*, if it stays invariant when we flip the sign of $\mathcal{C}$, or *odd*, if it changes sign:

$$\omega|_{\mathcal{C}\to-\mathcal{C}} = \begin{cases} \omega \,, & \text{if } \omega \text{ is } \textit{even} \text{ w.r.t. } \mathcal{C} \,, \\ -\omega \,, & \text{if } \omega \text{ is } \textit{odd} \text{ w.r.t. } \mathcal{C} \,. \end{cases} \tag{3.8}$$

For a logarithmic one-form $\mathrm{d}\log W$, this definition implies that the letter W is even (odd) with respect to a square root $\mathcal{C}$ if $W|_{\mathcal{C}\to-\mathcal{C}} = W$ ($W|_{\mathcal{C}\to-\mathcal{C}} = 1/W$). For example, a typical odd letter has the form

$$\frac{A+\mathcal{C}}{A-\mathcal{C}} \,, \tag{3.9}$$

where $\mathcal{C}$ is square root and A is a rational function. The fact that all one-forms appearing in the DEs for the MIs have a well-defined transformation under the change of the sign of the square roots follows from the way the square roots enter in the definition of the MIs. The scalar integrals, i.e. the integrals of the form $I^{(F),a_9,a_{10},a_{11}}_{a_1,\ldots,a_8}$, are by definition even with respect to all square roots. The square roots enter the game in the construction of MIs which satisfy DEs in the canonical form. As we will see later in this section (e.g. see eq. (3.15)), the square roots appear as overall normalisation of the MIs. More explicitly, each MI $\mathcal{I}$ has the form

$$\mathcal{I}(\vec{x},\varepsilon) = \mathcal{C}(\vec{x}) \sum_i c_i(\vec{x},\varepsilon) \, I_i(\vec{x},\varepsilon) \,, \tag{3.10}$$

where $\mathcal{C}(\vec{x})$ is either 1 or a product of square roots, $c_i(\vec{x},\varepsilon)$ are rational functions, and I_i are scalar integrals. This way, the MIs gain a charge with respect to the square roots,

JHEP07(2024)073

and the entries of the connection matrices — and thus the one-forms — inherit it from the MIs. With a slight abuse of notation, we say that a MI or one-form has charge $\mathcal{C}$ if it is odd with respect to $\mathcal{C}$.

In order to construct a basis of MIs which satisfies DEs of the previous forms, we used the approach outlined in ref. [19]. For completeness, we briefly summarise it in the following. It is a bottom-up approach, i.e. we start from the integral sectors with the fewest number of propagators, and we bring the DEs to the desired form sector by sector. The simplification of the DEs is done by following a procedure which exploits a set of heuristic criteria and draws as much as possible from known results in the literature. In particular, we perform the following steps. Let S be a sector of topology F.

- **Step 1**: we choose candidate MIs $\vec{\mathcal{L}}_{F,S}(\vec{x},\varepsilon)$ for sector S by requiring that the homogeneous DE[2] has the ε structure

$$\mathrm{d}\,\vec{\mathcal{L}}_{F,S}(\vec{x},\varepsilon) = \sum_{k=0}^{k_{\max}} \varepsilon^k \mathrm{d}\tilde{A}^{(F,S)}_{k,\mathrm{Hom}}(\vec{x}) \cdot \vec{\mathcal{L}}_{F,S}(\vec{x},\varepsilon) + (\text{sub-sectors})\,, \tag{3.11}$$

  where $k_{\max} = 2$ for the elliptic sector in PB_B, otherwise $k_{\max} = 1$. We neglect all contributions from the sub-sectors, which constitute the inhomogeneous terms of the DEs. As a guiding principle, we select MI candidates following patterns observed in previously studied cases. Since in this step we are mostly interested in the ε structure of DEs for the candidate MIs under study, we exploit finite fields technique to perform IBP reduction and to reconstruct the DEs on a univariate ε-slice, i.e. we set to numbers all the kinematic invariants and reconstruct just the analytic dependence in ε.

- **Step 2**: we reconstruct analytically the homogeneous DEs. Except for the two problematic sectors shown in figure 2, which we will discuss later, we construct a rational transformation such that the DEs take the intermediate form

$$\mathrm{d}\,\vec{\mathcal{J}}_{F,S}(\vec{x},\varepsilon) = \left(\mathrm{d}\hat{A}^{(F,S)}_{0,\mathrm{Hom}}(\vec{x}) + \varepsilon\,\mathrm{d}\hat{A}^{(F,S)}_{1,\mathrm{Hom}}(\vec{x})\right) \cdot \vec{\mathcal{J}}_{F,S}(\vec{x},\varepsilon) + (\text{sub-sectors})\,, \tag{3.12}$$

  where $\hat{A}^{(F,S)}_{0,\mathrm{Hom}}$, and $\hat{A}^{(F,S)}_{1,\mathrm{Hom}}$ are matrices of rational functions, and $\hat{A}^{(F,S)}_{0,\mathrm{Hom}}$ is diagonal and non-zero only in correspondence of the MIs which require a square-root normalisation. This enables the straightforward use of finite fields techniques in the reconstruction of DEs [26].

We perform the previous steps sector by sector, starting from the lower sectors and going up to the top sectors. Finally, we proceed with the last step.

- **Step 3**: we reconstruct analytically the DEs, this time including also the sub-sectors contributions, with respect to the basis $\vec{\mathcal{J}}_F = \cup_S \vec{\mathcal{J}}_{F,S}$, once again keeping the square roots out of the computation. While for most of the sectors the previous steps are

[2]Given an integral sector, the homogeneous DE is the subset of a DE which contains the contributions coming only from the integrals of that sector. The corresponding connection matrix is zero everywhere except for the diagonal square block corresponding to the MIs of the chosen sector. As a consequence, since all the sub-topologies do not contribute to it, the maximal cut of a certain MI is also a solution to the homogeneous DEs of the corresponding sector [117].

JHEP07(2024)073

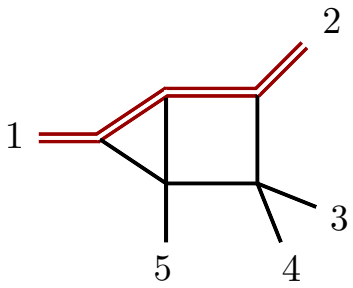

(a) The elliptic sector which we refer to as $321B$.

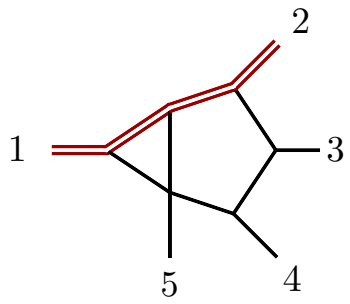

(b) Pentagon-triangle sector containing a nested square root. We refer to it as $421B$.

Figure 2. 'Problematic' sectors of topology PB_B.

enough to ensure that also the sub-sectors part of the DEs is in ε-factorised form, we found that some integral sectors need further adjustments. In this case, in order to achieve an ε-factorised form, it is sufficient to modify the definition of the MIs in the sector by including appropriate linear combination of the MIs of the sub-sectors which are not in ε-factorised form. The specific form of the linear combinations is fixed by demanding that the DEs are ε-factorised off diagonal (e.g. see [118]).

As a result, we obtain DEs whose connection matrices are rational, ε-factorised off diagonal, and linear in ε on the diagonal. The ε-factorised form can then be obtained via the rotation $\vec{\mathcal{I}}_F = N_F(\vec{x}) \cdot \vec{\mathcal{J}}_F$, as

$$\mathrm{d}\,\vec{\mathcal{I}}_F(\vec{x},\varepsilon) = \varepsilon \left(N_F(\vec{x}) \cdot \mathrm{d}\widehat{A}^{(F)}_{1,\mathrm{Hom}}(\vec{x}) \cdot N_F^{-1}(\vec{x}) \right) \cdot \vec{\mathcal{I}}_F(\vec{x},\varepsilon)\,, \tag{3.13}$$

where $N_F(\vec{x})$ is a diagonal matrix which captures all square-root normalisations and satisfies

$$\mathrm{d}\widehat{A}^{(F)}_{0,\mathrm{Hom}} + N_F^{-1} \cdot \mathrm{d}N_F = 0\,. \tag{3.14}$$

Through the strategy described above, we built a basis of MIs for topology PB_C which satisfies the DEs in canonical form. Contrarily, such a form is not possible for topology PB_B. Two sectors, shown in figure 2, present additional challenges. These can be identified by analysing the factorisation properties of the Picard-Fuchs operators [119, 120]. The sectors in figure 2 are in fact the only ones whose MIs have Picard-Fuchs operators with irreducible factors of degree 2, in contrast with all the other MIs, whose Picard-Fuchs operators factorise into linear factors. We devote sections 3.3 and 3.5 to a thorough analysis of these sectors, and summarise here the main conclusions. By analysing the homogeneous DEs for the sector in figure 2(a), we find that their solution involves elliptic integrals. While the last few years have seen important progress in the construction of ε-factorised DEs beyond the standard '$\varepsilon \times \mathrm{d}\log$' case in eqs. (3.4) and (3.5) [83, 84, 121], this problem is challenging in general. Moreover, the transformation required to achieve an ε-factorised form in this case involves transcendental functions (such as elliptic ones). This feature adds a further level of complexity for the numerical evaluation. In other words, even if an ε-factorised form of the DEs could be obtained in this case, the numerical evaluation of the solution would remain an open

JHEP07(2024)073

problem. The most common approach in such cases is to resort to semi-numerical methods such as the generalised power series expansion, which can be equally applied even without an ε-factorised form. Nonetheless, we put some effort into choosing MIs for this sector such that the connection matrices are polynomial in ε up to order ε^2, and all the entries which do not involve MIs of the two problematic sectors are ε-factorised. With respect to the generic form, this makes the expression of the DEs more compact, and improves the evaluation time of the solution using generalised power series expansions.

The second problematic sector, shown in figure 2(b), can be put into ε-factorised form, but at the cost of introducing a nested square root, similar to the one encountered in ref. [74]. While in principle this is not a problem, in practice the available codes implementing the generalised power series expansion method cannot handle a nested square root. For this reason, we prefer to omit this transformation, and adopt a basis of 3 MIs for this sector such that the connection matrices have a 2×2 block with non-zero ε^0 terms.

In light of the previous considerations, we built a basis of MIs for topology PB_B which satisfies a system of DEs as in eq. (3.2) with the connection matrix $\mathrm{d}A^{(\text{PB}_B)}$ of the form given in eq. (3.6) with $k_{\max} = 2$. Only the 27 entries of the connection matrix which couple the differential of $\mathcal{I}_{\text{PB}_B,37}$ to MIs other than itself are quadratic in ε. These entries depend on a subset of the kinematic invariants (see section 3.5). The entries which are instead non-zero at $\varepsilon = 0$ are 16. Of these, 4 involve the MIs $\mathcal{I}_{\text{PB}_B,19}$ and $\mathcal{I}_{\text{PB}_B,20}$, and can be eliminated as discussed in section 3.3 at the cost of introducing a nested square root. The remaining entries involve at least one of the MIs of the elliptic sector (see section 3.5).

Before we move on to discussing the choice of MIs for the most complicated sectors, we remark that another important aspect in the construction of the integral bases is to minimise both the highest numerator rank and the quantity of dotted propagators. This requirement is crucial in order to prevent the size and number of IBP relations needed from exploding and thus making the calculation computationally too expensive. To further ameliorate this aspect, we used the software NeatIBP [90] to generate optimised IBP relations through the solution of syzygy equations [91].

3.1 Pentagon-box sectors

The eight-propagator pentagon-box sectors shown in figures 1(b) and 1(c) contain three MIs for topology PB_B and four MIs for topology PB_C.

Regarding topology PB_B, since the number of MIs is the same as in the easier mass configurations, we then find that a canonical basis of MIs for this sector is [20]

$$\begin{aligned}
\mathcal{I}_{\text{PB}_B,1} &= \varepsilon^4\, d_{15}\ \mathrm{tr}_5\, I^{(\text{PB}_B),[12],0,0,0}_{1,1,1,1,1,1,1,1,1}\,, \\
\mathcal{I}_{\text{PB}_B,2} &= \varepsilon^4\, d_{15}\ \mathrm{tr}_5\, I^{(\text{PB}_B),[11],0,0,0}_{1,1,1,1,1,1,1,1,1}\,, \\
\mathcal{I}_{\text{PB}_B,3} &= \varepsilon^4\, d_{15}\, d_{23}\, d_{34} \left(I^{(\text{PB}_B),1,0,0}_{1,1,1,1,1,1,1,1,1} + m_t^2\, I^{(\text{PB}_B),0,0,0}_{1,1,1,1,1,1,1,1,1} \right) .
\end{aligned} \tag{3.15}$$

From numerical evaluations with AMFlow we observe that $\mathcal{I}_{\text{PB}_B,1}$ vanishes up to order ε^4.

Topology PB_C instead has four MIs in the top sector. We choose the first three similarly to topology PB_B. The construction of the fourth MI is more complicated. We start from the scalar integral in $d = 6 - 2\varepsilon$ dimensions, expressed in terms of integrals in $d = 4 - 2\varepsilon$

JHEP07(2024)073

dimensions using LiteRed's implementation of the dimension-shifting relations [122]. With this choice, the DEs are linear in ε. We then construct a transformation of the fourth MI to eliminate the ε^0 terms. The resulting expression is however complicated, has rank-4 numerators, and involves a spurious pole. We then search for a representation of this MI which is free of these undesirable features by fitting an ansatz made of (at most) rank-2 integrals on the top sector. This resulted in the following choices:

$$\begin{aligned}
\mathcal{I}_{\mathrm{PB}_C,1} &= \varepsilon^4\; d_{34}\, d_{45}\left(d_{12}+m_t^2\right) I^{(\mathrm{PB}_C),1,0,0}_{1,1,1,1,1,1,1,1,1}\,,\\
\mathcal{I}_{\mathrm{PB}_C,2} &= \varepsilon^4\; \mathrm{tr}_5\,(d_{12}+m_t^2)\, I^{(\mathrm{PB}_C),[11],0,0,0}_{1,1,1,1,1,1,1,1,1}\,,\\
\mathcal{I}_{\mathrm{PB}_C,3} &= \varepsilon^4\; \mathrm{tr}_5\,(d_{12}+m_t^2)\, I^{(\mathrm{PB}_C),[12],0,0,0}_{1,1,1,1,1,1,1,1,1}\,,\\
\mathcal{I}_{\mathrm{PB}_C,4} &= \varepsilon^4\,\frac{\beta_{12}}{\mathrm{tr}_5}\,4\,d_{34}d_{45}(d_{12}+m_t^2)\big[(d_{45}-d_{12}-m_t^2)I^{(\mathrm{PB}_C),1,0,1}_{1,1,1,1,1,1,1,1,1}-d_{34}d_{45}I^{(\mathrm{PB}_C),1,0,0}_{1,1,1,1,1,1,1,1,1}+\\
&\qquad 2d_{23}(d_{12}+m_t^2)I^{(\mathrm{PB}_C),0,0,1}_{1,1,1,1,1,1,1,1,1}+(\text{sub-sectors})\big]\,.
\end{aligned} \tag{3.16}$$

The sub-sector terms in $\mathcal{I}_{\mathrm{PB}_C,4}$ are rather lengthy, and can be found in the ancillary files [123]. Interestingly, numerical evaluations with AMFlow show that three of the four MIs of this sector ($\mathcal{I}_{\mathrm{PB}_C,2}$, $\mathcal{I}_{\mathrm{PB}_C,3}$ and $\mathcal{I}_{\mathrm{PB}_C,4}$) vanish up to order ε^4.

3.2 Double-box sectors

There are four double-box sectors, two in topology PB_B and two in topology PB_C, as shown in figure 3. The sectors (b), (c) and (d) in figure 3 have already been discussed in ref. [20]. Sector (a) of topology PB_B is instead new and contains six MIs. As for the pentagon-box sectors, we were able to construct compact expressions for some of the canonical MIs of this sector using μ_{ij} numerator insertions. The first three integrals ($\mathcal{I}_{\mathrm{PB}_B,4}$, $\mathcal{I}_{\mathrm{PB}_B,5}$ and $\mathcal{I}_{\mathrm{PB}_B,6}$) can be chosen as in sector (b) in figure 3 (see ref. [20]). Of the remaining three, we defined two ($\mathcal{I}_{\mathrm{PB}_B,7}$ and $\mathcal{I}_{\mathrm{PB}_B,8}$) using μ_{ij} numerators and dotted propagators:

$$\begin{aligned}
\mathcal{I}_{\mathrm{PB}_B,4} &= \varepsilon^4\, d_{15}\, d_{23}\,(d_{12}+m_t^2) I^{(\mathrm{PB}_B),0,0,0}_{1,1,1,0,1,1,1,1}\,,\\
\mathcal{I}_{\mathrm{PB}_B,5} &= \varepsilon^4\, d_{15}\, d_{23}\,\left(I^{(\mathrm{PB}_B),0,1,0}_{1,1,1,0,1,1,1,1}+m_t^2\, I^{(\mathrm{PB}_B),0,0,0}_{1,1,1,0,1,1,1,1}\right)\,,\\
\mathcal{I}_{\mathrm{PB}_B,6} &= \varepsilon^4\;\mathrm{tr}_5\,\left(I^{(\mathrm{PB}_B),[12],0,0,0}_{1,1,1,0,1,1,1,1}+(\text{sub-sectors})\right)\,,\\
\mathcal{I}_{\mathrm{PB}_B,7} &= \varepsilon^3\, d_{23}\;\mathrm{tr}_5\,\left(I^{(\mathrm{PB}_B),[12],0,0,0}_{1,1,2,0,1,1,1,1}+(\text{sub-sectors})\right)\,,\\
\mathcal{I}_{\mathrm{PB}_B,8} &= \varepsilon^3\, d_{15}\;\mathrm{tr}_5\; I^{(\mathrm{PB}_B),[12],0,0,0}_{1,1,1,0,1,1,2,1}\,.
\end{aligned} \tag{3.17}$$

From numerical evaluations with AMFlow, we observe that $\mathcal{I}_{\mathrm{PB}_B,6}$ is zero up to order ε^4. For the sixth MI of this sector ($\mathcal{I}_{\mathrm{PB}_B,9}$), we could not find a compact representation. We started from the derivative of $\mathcal{I}_{\mathrm{PB}_B,4}$ with respect to d_{23}, which leads to a linear dependence of the connection matrices on ε. We then constructed a transformation to eliminate the ε^0 part of the connection matrices, both in the homogeneous part of the DEs and in the sub-sectors. This constraint amounts to first-order DEs for the entries of the transformation matrix, which we could solve in terms of rational functions. The resulting expression for $\mathcal{I}_{\mathrm{PB}_B,9}$ is rather lengthy, and can be found in the ancillary files [123] together with the sub-sector terms of $\mathcal{I}_{\mathrm{PB}_B,6}$ and $\mathcal{I}_{\mathrm{PB}_B,7}$.

JHEP07(2024)073

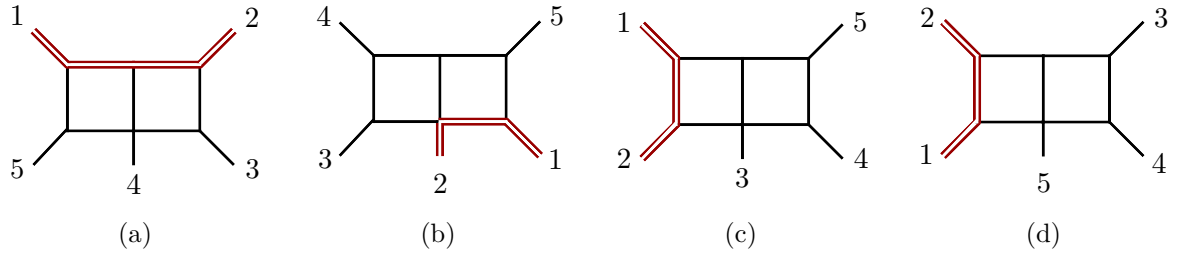

Figure 3. The four five-point double-box topologies covering the MIs $\mathcal{I}_{\mathrm{PB}_B,4}$ – $\mathcal{I}_{\mathrm{PB}_B,9}$ (a), $\mathcal{I}_{\mathrm{PB}_B,10}$ – $\mathcal{I}_{\mathrm{PB}_B,12}$ (b), $\mathcal{I}_{\mathrm{PB}_C,5}$ – $\mathcal{I}_{\mathrm{PB}_C,8}$ (c) and $\mathcal{I}_{\mathrm{PB}_C,15}$ – $\mathcal{I}_{\mathrm{PB}_C,18}$ (d) respectively.

3.3 Pentagon-triangle sector: a nested square root

There is only one pentagon-triangle sector, shown in figure 2(b) and dubbed $421B$, and it appears in topology PB_B. This sector has not been studied previously in the literature and contains three MIs. One MI can be chosen to take the same form as in the analogous topology of the five-point integrals with an off-shell leg and massless internal propagators [35]. For the remaining two integrals, we made use of numerator structures inspired by local numerators [108] and written in terms of Dirac traces, as

$$\begin{aligned}
\mathcal{I}_{\mathrm{PB}_B,18} &= \varepsilon^4\ \mathrm{tr}_5\ I^{(\mathrm{PB}_B),[11],0,0,0}_{1,1,1,1,1,1,0,1}\,, \\
\mathcal{I}_{\mathrm{PB}_B,19} &= \varepsilon^4\, d_{45}\, I^{(\mathrm{PB}_B),0,0,0}_{1,1,1,1,1,1,0,1} \left[\mathrm{tr}(\gamma_5 \not{p}_3(\not{k}_1 - \not{p}_2 - \not{p}_3)\not{p}_4\not{p}_2)\right]\,, \\
\mathcal{I}_{\mathrm{PB}_B,20} &= \varepsilon^4\, d_{45}\, I^{(\mathrm{PB}_B),0,0,0}_{1,1,1,1,1,1,0,1} \left[\mathrm{tr}(\not{p}_3(\not{k}_1 - \not{p}_2 - \not{p}_3)\not{p}_4\not{p}_2)\right]\,,
\end{aligned} \tag{3.18}$$

where the terms in the square brackets are meant to be taken under the integral sign. Note that the numerators in $\mathcal{I}_{\mathrm{PB}_B,19}$ and $\mathcal{I}_{\mathrm{PB}_B,20}$ are the parity even and odd parts of the spinor chain $\langle 3|k_1 - p_2 - p_3|4]$, multiplied by an arbitrary factor of $\langle 42\rangle[23]$ to cancel the helicity little-group scaling. From numerical evaluations with AMFlow, we observe that $\mathcal{I}_{\mathrm{PB}_B,19}$ and $\mathcal{I}_{\mathrm{PB}_B,20}$ start at order ε^4, whereas $\mathcal{I}_{\mathrm{PB}_B,18}$ vanishes up to order ε^4.

The choice of Dirac trace in the numerator is made in order to cancel the potential singularity as the propagator momentum $k_1 - p_2 - p_3$ becomes collinear to either adjacent massless leg p_3 or p_4. The two simple numerator structures that can achieve this are $\langle 3|k_1 - p_2 - p_3|4]$ and its spinor conjugate $\langle 4|k_1 - p_2 - p_3|3]$. Setting these objects inside a trace ensures they are free from any spinor phases. We choose $\mathrm{tr}_\pm[\not{p}_3(\not{k}_1 - \not{p}_2 - \not{p}_3)\not{p}_4\not{p}_2]$, which have the same loop-momentum dependence but different normalisation. It is then useful to split into parity odd and even pieces by taking linear combinations. One can also write an alternative version of this 'local' numerator as $(l - l^*)^2$, where $l = k_1 - p_2 - p_3$ and l^* solves the quadruple cut constraints

$$\{(l^*)^2 = 0\,,\ (l^* - p_4)^2 = 0\,,\ (l^* + p_3)^2 = 0\,,\ (l^* + p_2 + p_3)^2 = m_t^2\}\,. \tag{3.19}$$

As discussed in section 2, we remove the parity degree of freedom and replace the parity-odd trace with the parity-even square root tr_5 defined in eq. (2.18).

JHEP07(2024)073

With the MIs in eq. (3.18), the homogeneous DEs for this sector are linear in ε, but not ε-factorised. They take the form

$$\mathrm{d}\,\mathcal{I}_{421B} = \left[\begin{pmatrix} 0 & 0 & 0 \\ 0 & X & Y \\ 0 & Y & X \end{pmatrix} + \mathcal{O}(\varepsilon)\right] \cdot \mathcal{I}_{421B} + (\text{sub-sectors})\,, \qquad \mathcal{I}_{421B} = \begin{pmatrix} \mathcal{I}_{\mathrm{PB}_B,18} \\ \mathcal{I}_{\mathrm{PB}_B,19} \\ \mathcal{I}_{\mathrm{PB}_B,20} \end{pmatrix}. \tag{3.20}$$

The omitted terms in the square brackets are proportional to ε. All sub-sector terms are ε-factorised, except for the entries coupling $\mathcal{I}_{\mathrm{PB}_B,19}$ and $\mathcal{I}_{\mathrm{PB}_B,20}$ to the elliptic sector ($\mathcal{I}_{\mathrm{PB}_B,i}$ for $i = 35, 36, 37$). As anticipated in the introduction to this section, the factorisation of ε in the entire diagonal block requires a transformation involving a nested square root.

The higher complexity of this sector can be detected by analysing the corresponding Picard-Fuchs operators as proposed in ref. [120]. First, we reduce the multi-scale problem to a single-scale one by defining a univariate phase-space slice,

$$x_i = a_i + b_i\,\lambda\,, \qquad \forall\, i = 1, \ldots, 6\,, \tag{3.21}$$

with $a_i, b_i \in \mathbb{Q}$, and viewing the MIs as functions of λ. The constants a_i and b_i in eq. (3.21) are chosen randomly, but one must make sure that no denominator factors of the connection matrices vanish on the univariate slice, so as to avoid singular points. Furthermore, we work modulo sub-topologies and modulo ε-corrections, i.e. we focus on the 3×3 block of the DEs corresponding to this sector and set $\varepsilon = 0$. The first MI of this sector, $\mathcal{I}_{\mathrm{PB}_B,18}$, decouples, as the corresponding DE-entries are already ε-factorised. In order to decouple $\mathcal{I}_{\mathrm{PB}_B,19}$ and $\mathcal{I}_{\mathrm{PB}_B,20}$ we need to differentiate one more time. In other words, the remaining 2×2 block is equivalent to a second-order ordinary differential equation in λ for each of the integrals separately:

$$L_i\,\mathrm{MaxCut}\,[\mathcal{I}_{\mathrm{PB}_B,i}]_{\varepsilon=0} = 0\,, \qquad L_i = \sum_{k=0}^{2} c_{i,k}(\lambda)\frac{\mathrm{d}^k}{\mathrm{d}\lambda^k}\,, \qquad \forall\, i = 19, 20\,. \tag{3.22}$$

The differential operators L_i which annihilate the MIs are called Picard-Fuchs operators. The factorisation properties of the Picard-Fuchs operators encode useful information for the factorisation of ε. Whenever they factor completely into linear factors, the strategy of ref. [120] allows one to construct a transformation which puts the DEs in ε-factorised form. The Picard-Fuchs operators of $\mathcal{I}_{\mathrm{PB}_B,19}$ and $\mathcal{I}_{\mathrm{PB}_B,20}$ are however second-order and irreducible.[3] The appearance of an irreducible factor of order greater than one in the factorisation of a Picard-Fuchs operator is an indication that the Feynman integral cannot be expressed in terms of MPLs [125]. In this case, however, we find that the solutions to the Picard-Fuchs equations in eq. (3.22) — equivalently, the solution to the homogeneous DEs for this block — do not contain elliptic integrals, but rather a nested square root. Indeed, we can actually put the DEs in ε-factorised form with an algebraic change of basis, as we discuss below. It may therefore be possible to factor these Picard-Fuchs operators into linear factors by allowing for algebraic functions in the coefficients. In section 3.5 we will see that also the

[3] We used the Maple command `DFactor` to factorise the differential operators [124]. Note that this algorithm factors into differential operators with rational function coefficients, and may therefore miss factorisations involving algebraic coefficients.

JHEP07(2024)073

Picard-Fuchs operators of the integrals of the sector shown in figure 2(a) contain second-order irreducible factors. In that case we will however find elliptic integrals in the solutions. The Picard-Fuchs operators (modulo ε corrections and sub-sectors) for all the other MIs of both topology PB_B and PB_C are instead first-order.

We now proceed to put the homogeneous DEs for this sector in ε-factorised form. Thanks to the particularly symmetric form of the 2×2 ε^0 block corresponding to $\mathcal{I}_{\mathrm{PB}_B,19}$ and $\mathcal{I}_{\mathrm{PB}_B,20}$ (see eq. (3.20)), the off-diagonal non-zero entries can be removed by simply replacing these MIs by their sum and difference, i.e.

$$\mathcal{I}_{421B} \quad \longrightarrow \quad \mathcal{I}'_{421B} = T_1 \cdot \mathcal{I}_{421B}\,, \qquad T_1 = \begin{pmatrix} 1 & 0 & 0 \\ 0 & 1 & 1 \\ 0 & 1 & -1 \end{pmatrix}. \tag{3.23}$$

Note that this transformation mixes integrals of different tr_5-charge ($\mathcal{I}_{\mathrm{PB}_B,19}$ is even, $\mathcal{I}_{\mathrm{PB}_B,20}$ is odd), and gives $\langle 3|(k_1-p_2-p_3)42|3]$ and its parity conjugate as numerators for $\mathcal{I}'_{\mathrm{PB}_B,19}$ and $\mathcal{I}'_{\mathrm{PB}_B,20}$. The resulting homogeneous DEs have non-zero ε^0 terms only on the diagonal, which can thus be removed by proper normalisation. The required normalisation factors are reciprocal of the solutions to the Picard-Fuchs equations in eq. (3.22), and involve a nested square root:

$$N_\pm = \frac{\sqrt{n_\pm}}{d_{45}\, r_2}\,, \tag{3.24}$$

where

$$n_\pm = d_{23}^2\,\mathrm{tr}_5^2 - 8 r_2 r_4 \pm 4 d_{23} r_3\,\mathrm{tr}_5\,, \tag{3.25}$$

with

$$\begin{aligned}
r_2 &= 2d_{23}(d_{23}+d_{34}-d_{15})+d_{34}m_t^2\,,\\
r_3 &= d_{23}\left[d_{12}(d_{23}-d_{15})-d_{23}d_{34}+(d_{34}-d_{15})d_{45}\right]+\left[d_{23}(d_{15}-d_{23}-2d_{34})+\ d_{34}d_{45}\right]m_t^2-d_{34}m_t^4\,,\\
r_4 &= 2d_{12}d_{15}d_{23}d_{45}+\left[2d_{12}d_{23}(d_{23}-d_{15})-d_{34}(2d_{23}^2-2d_{23}d_{45}+d_{45}^2)\right]m_t^2+\\
&\quad\ 2(d_{23}^2+d_{34}d_{45}-d_{15}d_{23})m_t^4\,.
\end{aligned} \tag{3.26}$$

We emphasise that $n_\pm$ involves the square root tr_5, and that n_+ and n_- are related by swapping the sign of tr_5. While the expression of the normalisation factors in eq. (3.24) is fairly intricate, it is straightforward to verify that they do not introduce spurious singularities. In other words, the product n_+n_- factorises in terms of the same factors present in the denominators of the connection matrices prior to the transformation. Furthermore, we note that the factorisation of expressions involving square roots is not unique, and therefore a simpler representation of these normalisation factors may exist. In particular, we find that this nested square root can also be written compactly in terms of traces of gamma matrices,

$$N_\pm = \sqrt{8\left(\frac{\mathrm{tr}_\mp(\not{p}_3\not{p}_2\not{p}_{12}\not{p}_5)}{\mathrm{tr}_\mp(\not{p}_4\not{p}_5\not{p}_3\not{p}_2)}+\frac{4m_t^2}{s_{45}}\right)\frac{\mathrm{tr}_\mp(\not{p}_3\not{p}_2\not{p}_{12}\not{p}_5)}{\mathrm{tr}_\mp(\not{p}_4\not{p}_5\not{p}_3\not{p}_2)}}\,, \tag{3.27}$$

JHEP07(2024)073

in which it is clear that the interior square root could be rationalised when using a momentum-twistor representation [19, 126] with rational parameterisations for the spinor products, and that the argument of the outer square root becomes a perfect square in the massless limit. We have checked that $n_\pm$ cannot be expressed as a perfect square of the form $(a+b\,\mathrm{tr}_5)^2$, for some rational functions a and b, which would allow us to remove the exterior square root. Finally, the normalisation factors in eq. (3.24) do not have well-defined behaviour under swapping the sign of tr_5. It is instead desirable that all MIs are either even or odd with respect to this operation. We therefore apply another transformation of the form of eq. (3.23) to restore this property. In conclusion, the basis of this sector which puts the DEs in ε-factorised form is

$$\mathcal{I}''_{421B} = \begin{pmatrix} 1 & 0 & 0 \\ 0 & 1 & 1 \\ 0 & 1 & -1 \end{pmatrix} \cdot \begin{pmatrix} 1 & 0 & 0 \\ 0 & N_+ & 0 \\ 0 & 0 & N_- \end{pmatrix} \cdot \begin{pmatrix} 1 & 0 & 0 \\ 0 & 1 & 1 \\ 0 & 1 & -1 \end{pmatrix} \cdot \mathcal{I}_{421B}\,. \tag{3.28}$$

Keeping in mind that we did not put in ε-factorised form the elliptic sector (see section 3.5), and that DiffExp cannot handle nested square roots, we prefer to omit this transformation from our chosen basis of MIs.

3.4 Pentagon-bubble sectors

There are two sectors in the form of a pentagon with a bubble insertion, shown in figure 4: one in topology PB_B, with two MIs, and one in topology PB_C, with three MIs. Both sectors present a new mass configuration. However, since the number of MIs for the pentagon-bubble integrals in topology PB_B is the same as in previously studied cases, we can make a similar choice for the canonical basis:

$$\begin{aligned} \mathcal{I}_{\mathrm{PB}_B,45} &= \varepsilon^3\ \mathrm{tr}_5\ I^{(\mathrm{PB}_B),[11],0,0,0}_{1,1,1,1,0,1,0,2}\,, \\ \mathcal{I}_{\mathrm{PB}_B,46} &= \varepsilon^3(1-2\varepsilon)\,d_{23}\,d_{34} I^{(\mathrm{PB}_B),0,0,0}_{1,1,1,1,0,1,0,1}\,. \end{aligned} \tag{3.29}$$

Regarding the pentagon-bubble sector in topology PB_C, we find a canonical basis where all three MIs involve dotted propagators:

$$\begin{aligned} \mathcal{I}_{\mathrm{PB}_C,32} &= \varepsilon^3\ \mathrm{tr}_5\ I^{(\mathrm{PB}_C),[11],0,0,0}_{1,1,1,1,0,2,0,1}\,, \\ \mathcal{I}_{\mathrm{PB}_C,33} &= \varepsilon^3\ \mathrm{tr}_5\ I^{(\mathrm{PB}_C),[11],0,0,0}_{1,1,1,1,0,1,0,2}\,, \\ \mathcal{I}_{\mathrm{PB}_C,34} &= \varepsilon^3\,d_{34}\,d_{45}\left(I^{(\mathrm{PB}_C),1,0,0}_{1,1,1,1,0,2,0,1} + m_t^2 I^{(\mathrm{PB}_C),0,0,0}_{1,1,1,1,0,2,0,1}\right)\,. \end{aligned} \tag{3.30}$$

3.5 Elliptic sector

The most complicated sector belongs to topology PB_B and is shown in figure 2(a). It is a four-point sector, and thus its integrals depends on four variables only (d_{12}, d_{34}, d_{15} and m_t^2). There are 3 MIs, which we choose as

$$\begin{aligned} \mathcal{I}_{\mathrm{PB}_B,35} &= \varepsilon^4\,d_{15}\,(d_{12}+m_t^2)\,I^{(\mathrm{PB}_B),0,0,0}_{1,1,0,1,1,1,0,1}\,, \\ \mathcal{I}_{\mathrm{PB}_B,36} &= \varepsilon^4\,\sqrt{(d_{15}-d_{34})^2-2d_{34}m_t^2}\,I^{(\mathrm{PB}_B),0,0,0}_{1,1,0,1,1,1,0,1}\,[2k_1\cdot p_1]\,, \\ \mathcal{I}_{\mathrm{PB}_B,37} &= \varepsilon^4\,(-1+2\varepsilon)\,d_{15}\,I^{(\mathrm{PB}_B),0,0,0}_{1,1,0,1,1,1,0,1}\,[2k_2\cdot p_2]\,, \end{aligned} \tag{3.31}$$

JHEP07(2024)073

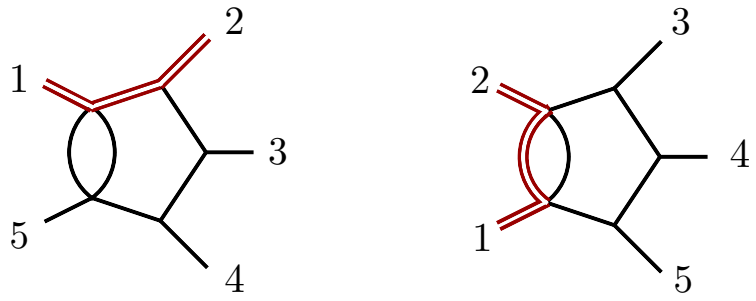

Figure 4. The two pentagon-bubble sectors for topologies PB_B (sub-figure (a)) and PB_C (sub-figure (b)).

where we recall that the terms in the square brackets are meant to be taken under the integral sign. From numerical evaluations with AMFlow, we observe that the chosen MIs of this sector are non-zero only starting from order ε^4. While the DEs for this sector are not ε-factorised, the MIs above simplify them substantially with respect to an arbitrary choice. The normalisation factor of $\mathcal{I}_{\mathrm{PB}_B,36}$ is chosen so as to factorise ε in the corresponding diagonal entry of the DEs. The factor of $(-1+2\varepsilon)$ in $\mathcal{I}_{\mathrm{PB}_B,37}$ is inserted to remove all ε-dependent factors from the denominators of the connection matrices. The remaining kinematic-dependent normalisation factors of $\mathcal{I}_{\mathrm{PB}_B,35}$ and $\mathcal{I}_{\mathrm{PB}_B,37}$ ensure that all MIs in the basis have the same dimensionality, and are chosen heuristically as they lead to more compact connection matrices. The DEs have the following structure:

$$\mathrm{d}\,\mathcal{I}_{321B} = \begin{pmatrix} *+\varepsilon* & \varepsilon* & * \\ *+\varepsilon* & \varepsilon* & * \\ (1-2\varepsilon)(*+\varepsilon*) & (1-2\varepsilon)\varepsilon* & *+\varepsilon* \end{pmatrix} \cdot \mathcal{I}_{321B} + (\text{sub-sectors})\,, \quad (3.32)$$

where $\mathcal{I}_{321B} = (\mathcal{I}_{\mathrm{PB}_B,35}, \mathcal{I}_{\mathrm{PB}_B,36}, \mathcal{I}_{\mathrm{PB}_B,37})^\top$, and each asterisk denotes a distinct one-form. The sub-sectors follow the same pattern as the diagonal block shown above: the entries coupling $\mathcal{I}_{\mathrm{PB}_B,35}$ and $\mathcal{I}_{\mathrm{PB}_B,36}$ to the sub-sectors are linear in ε, while for $\mathcal{I}_{\mathrm{PB}_B,37}$ they are quadratic.

The analysis of the Picard-Fuchs operators L_i allows us to better characterise the complexity of this sector. Following the procedure outlined in section 3.3, we construct the differential operators L_i such that

$$L_i\,\mathrm{MaxCut}\,[\mathcal{I}_{\mathrm{PB}_B,i}]_{\varepsilon=0} = 0\,, \qquad L_i = \sum_{k=0}^{r_i} c_{i,k}(\lambda)\frac{\mathrm{d}^k}{\mathrm{d}\lambda^k}\,, \qquad \forall\, i = 35,36,37\,, \quad (3.33)$$

with $r_{35} = r_{37} = 2$ and $r_{36} = 3$. We recall that we work on a random univariate phase-space slice (see eq. (3.21)), modulo sub-sectors and ε-corrections. L_{35} and L_{37} are second-order, irreducible operators. The solution to L_{35} involves the elliptic integral of the first kind $\mathrm{K}(x)$, while the solution to L_{37} also contains derivatives of the latter.[4] L_{36} is instead third-order,

[4]We obtained the solutions to the second-order Picard-Fuchs operators with the Maple command `hypergeometricsols`. We thank Christoph Dlapa for suggesting this.

JHEP07(2024)073

and factorises into the product of a second- and a first-order operator. The first-order factor is simply $\mathrm{d}/\mathrm{d}\lambda$, which follows from the fact that the reciprocal of the chosen normalisation factor of $\mathcal{I}_{\mathrm{PB}_B,36}$ is a solution to L_{36}. In appendix A we determine the elliptic curve underlying the elliptic integrals appearing in this analysis, and identify the solutions to the Picard-Fuchs operator L_{35} with the periods of said elliptic curve.

4 'd log' and 'one-form' representation of the differential equations

Having obtained the connection matrices of the differential equations using the integral bases described in the previous sections, we present compact analytic expressions in terms of independent 'd log' and 'one-form' structures, as in eqs. (3.5) and (3.6). There are a variety of methods proposed in the literature to determine the alphabet of 'd log' forms where they exist. In our case, rather than constructing an ansatz of possible alphabet letters *a priori*, we first established a set of linearly independent one-forms organised according to the square root charges defined earlier in section 3. As discussed there, each entry of the connection matrices after the reconstruction is a rational function of the invariants, $\vec{x}$. We then add back the square root normalisations of each master integral to rotate the DEs into ε-factorised form (or as far as possible, in the case of topology PB_B). After this stage each entry takes the form

$$\begin{aligned} \mathrm{d}A_{ij}^{(F)}(\vec{x},\varepsilon) &= \sum_a \varepsilon^a \mathrm{d}A_{ij}^{(F),a}(\vec{x})\,, \\ \mathrm{d}A_{ij}^{(F),a}(\vec{x}) &= \mathcal{C}_{ij}^{(F)}(\vec{x}) \sum_{k=1}^{6} \mathrm{d}x_k\, f_{ijk}^{(F),a}(\vec{x})\,, \end{aligned} \tag{4.1}$$

where $\mathcal{C}_{ij}^{(F)}(\vec{x})$ are monomials in the possible square roots (including $\mathcal{C}_{ij}^{(F)}(\vec{x}) = 1$) that we have called charges (see section 3), and $f_{ijk}^{(F),a}$ are rational functions of the invariants $\vec{x}$. The sum over the orders in ε (index a) runs from 0 to 2 for PB_B, while PB_A and PB_C are in ε-factorised form (i.e., $a = 1$). There are 49 charges in total, with 23 appearing in the leading colour topologies.

At this stage, we determine the linear relations amongst each set of entries $\mathrm{d}A_{ij}^{(F),a}$ and of $\mathrm{d}\log W$'s that share the same charge $\mathcal{C}_{ij}^{(F)}$, where we use the notation W to indicate the letters of our alphabet. Since the square roots are an overall factor, we can divide them out and use finite field techniques to determine the linear relations. We then solve the linear relations by ordering with respect to the polynomial degree of the entries $\mathrm{d}A_{ij}^{(F),a}$ and preferring $\mathrm{d}\log$ structures. After iterating over all possible charges, all entries $\mathrm{d}A_{ij}^{(F),a}$ are expressed in terms $\mathrm{d}\log$ structures of our alphabet if possible (as in eq. (3.5)), and additionally a minimal set of simple one-forms otherwise (as in eq. (3.6), with some ω_i's being $\mathrm{d}\log$'s). For concreteness, we spell out the form of the connection matrix for PB_B:

$$\mathrm{d}A^{(\mathrm{PB}_B)}(\vec{x},\varepsilon) = \sum_{k=0}^{2} \varepsilon^k \left[\sum_i c_{k,i}^{(\mathrm{PB}_B)}\, \mathrm{d}\log\left(W_i(\vec{x})\right) + \sum_j d_{k,j}^{(\mathrm{PB}_B)}\, \omega_j(\vec{x}) \right], \tag{4.2}$$

where $c_{k,i}^{(\mathrm{PB}_B)}$ and $d_{k,j}^{(\mathrm{PB}_B)}$ are matrices of rational numbers. We stress that the $\mathrm{d}\log$'s are one-forms themselves, but in this context we call one-forms only those we could not express in

JHEP07(2024)073

terms of d log's. Furthermore, we emphasise that some of these one-forms are not closed, which implies they are not exact either.[5] In other words, they cannot be expressed as the differential of any function, let alone of a logarithm. Table 2 shows a summary of each topology.

The rational letters (i.e. those with $\mathcal{C}_{ij}^{(F)} = 1$) are easy to determine: they are the (algebraically independent) factors in the denominators of the connection matrices. Some of these letters are extremely simple, linear combinations of invariants, while others are high degree polynomials in the invariants $\vec{x}$ (up to degree 5). We determine that a large number of these high degree polynomials can be identified as Gram and Cayley determinants of the external kinematics. Others can be written in compact notation by using traces of gamma matrices. In total we find 58 rational letters for all one-loop and planar two-loop cases, although only 46 appear in the leading colour topologies.

The algebraic letters are all written in the manifestly odd form

$$\frac{A+\mathcal{C}}{A-\mathcal{C}}\,, \tag{4.3}$$

where $\mathcal{C}$ is one of the charges (apart from 1) and A is a rational function. There are a variety of methods proposed to determine the form of such letters, for example [73, 74, 127–129]. In our case, we were able to find all the required expressions by comparison with ansätze for the rational function A. Rather than printing the list of charges and letters here we present all the relevant definitions in the ancillary files [123] described in appendix C. In the case of $\mathcal{C} = \mathrm{tr}_5$, we find that compact representations can be found by using ratios of $\mathrm{tr}_+/\mathrm{tr}_-$ with arguments of either four or six gamma matrices. Explicit forms are given in the ancillary files, although this is only an aesthetic consideration.

In some cases, having found d log representations, we have subsequently imposed symmetries amongst the letters. This is particularly relevant for letters related to charges involving the three-mass triangle Gram determinants, $\Delta_{3,i}$. We note that the charge $\Delta_{3,4}$ appears in topologies PB_A and PB_C with 3 independent one-forms. We write the one-forms in terms of 4 letters in order to preserve these symmetries. This would be convenient in case one was looking for a set of special functions closed under permutations. In addition, for PB_A there are two additional letters containing tr_5 in our alphabet than independent entries of the connection matrix.

As a final remark, we notice that the mixed d log and one-form expression of the DEs for topology PB_B allows us to clearly separate the features in common with the standard canonical cases (PB_A and PB_C) from the new, more complicated ones. Moreover, it makes the expression of the DEs roughly 50 times more compact than if one stored the connection matrices separately for each derivative, as in the form generated by DiffExp for the semi-numerical solution. It would be interesting to find a way to exploit this simplification of the form of the DEs in the method of generalised power series expansions.

[5] A differential form ω is closed if $\mathrm{d}\omega = 0$. A one-form ω is exact if there exists a function f such that $\omega = \mathrm{d}f$. An exact form is thus by definition closed.

JHEP07(2024)073

topology	charges	d log letters	one-forms
PB_A	17	74	0
PB_B	16	72	63
PB_C	21	80	0
2-loop LC	23	98	63
P_A	8	41	0
P_B	10	45	0
P_C	17	55	0
P_D	29	64	0
1-loop	40	105	0

Table 2. Summary of the 'd log' and 'one-form' structures appearing in the differential equations for each topology, and cumulatively for all two-loop leading colour (LC) topologies and all 1-loop topologies. PB_A and PB_C contain three and one more letter than linearly independent entries of the connection matrices respectively. This is due to the imposed symmetries described in the text.

5 Numerical evaluation using generalised series expansions

In this section, we discuss the numerical evaluation of the master integrals. We obtain a semi-analytic solution to the system of differential equations associated with the master integrals by means of the method of generalised power series expansions [85], by exploiting the Mathematica package DiffExp [101]. We obtain the required boundary values numerically with the package AMFlow [102], which implements the auxiliary mass flow method [104–106]. We aim to evaluate the integrals in the physical scattering region relevant for phenomenology. We begin by defining this region. We then motivate our choice for the boundary point, and discuss a number of interesting features of the boundary values. Next, we present a number of checks we performed to validate our results. Finally, we comment on the performance of the numerical evaluation.

5.1 Physical scattering region

We restrict our analysis to the physical phase-space region corresponding to the s_{45} scattering channel ($45 \to 123$). All other $2 \to 3$ channels relevant for $t\bar{t}j$ production can be obtained from the s_{45} channel through suitable permutations of the momenta, and our numerical evaluation procedure can therefore be straightforwardly generalised to them as well. The s_{45} channel is defined by the following linear constraints on the kinematic invariants,

$$\begin{aligned} &p_1^2 > 0, \quad p_2^2 > 0, \quad p_4 \cdot p_5 > 0, \quad p_1 \cdot p_2 > 0, \quad p_1 \cdot p_3 > 0, \quad p_2 \cdot p_3 > 0, \\ &p_4 \cdot p_1 < 0, \quad p_4 \cdot p_2 < 0, \quad p_4 \cdot p_3 < 0, \quad p_5 \cdot p_1 < 0, \quad p_5 \cdot p_2 < 0, \quad p_5 \cdot p_3 < 0, \end{aligned} \tag{5.1}$$

complemented by the following higher-order constraints coming from Gram determinants,

$$\det G(p_i, p_j) < 0\,, \qquad \det G(p_i, p_j, p_k) > 0\,, \qquad \det G(p_i, p_j, p_k, p_l) < 0\,, \tag{5.2}$$

where i, j, k, l take distinct values in $\{1, \ldots, 5\}$. The Gram determinants involving two and four momenta give only one constraint each:

$$(d_{12} - m_t^2)(d_{12} + m_t^2) > 0\,, \qquad \mathrm{tr}_5^2 < 0\,. \tag{5.3}$$

JHEP07(2024)073

Those involving three momenta give a number of polynomial constraints on the kinematic invariants which we do not spell out. All constraints defining the s_{45} channel can be found in ancillary files [123].

5.2 Boundary values

The evaluation of the master integrals through the method of generalised power series expansions entails the integration of the DEs along a path connecting the target point with a starting point at which the values are known. We wish to confine such paths to the s_{45} channel in order to avoid analytic continuation, which is non-trivial to determine for multi-variable problems and increases the evaluation time. In this view, we choose a boundary point $\vec{x}_0$ in the s_{45} channel. The choice is arbitrary, but has an impact on the performance of the evaluation. We choose

$$\vec{x}_0 = \{2, 1, -1, 5, -2, 1\}\,, \tag{5.4}$$

following the criteria set in ref. [30], which we recall here.

1. The point $\vec{x}_0$ is invariant under the symmetries of the s_{45} channel, i.e. the exchanges of the external momenta $p_1 \leftrightarrow p_2$ and $p_4 \leftrightarrow p_5$.

2. The point $\vec{x}_0$ introduces a minimal number of distinct prime factors.

3. The point $\vec{x}_0$ lies on the spurious singularity $d_{23} + d_{34} = 0$.

The first two criteria reduce the number of independent transcendental constants in the values of the master integrals at $\vec{x}_0$. This is useful in view of a future analytic solution of the DEs. The second criterion also makes the numerical evaluation using AMFlow faster, as it reduces the number of prime fields required to reconstruct the DEs with respect to the auxiliary mass. We recall in fact that we interface AMFlow to FiniteFlow in order to solve the IBP relations over finite fields.

In order to understand the third criterion, we first need to define spurious singularities. A *spurious singularity* is a singularity of the connection matrix of the DEs which is not a singularity of the solution to the DEs once the boundary values are taken into account. The possible singularities of the MIs correspond to the factors in the denominators of the connection matrices. For DEs where a canonical 'd log form' is possible, this is equivalent to the rational letters of the alphabet. We find that two of them, $d_{23} + d_{34}$ and $d_{12} + d_{15} + m_t^2$, can vanish within the s_{45} channel.[6] By choosing the boundary point such that $d_{23} + d_{34} = 0$, we ensure that this spurious singularity is never crossed by a straight path starting from $\vec{x}_0$. This improves the speed of the integration with the generalised power series expansion methods, and is useful in view of a future solution in terms of one-fold integral representations along the lines of ref. [130]. We emphasise however that the presence of spurious singularities is not an obstacle for the generalised power series expansion method.

[6] We can prove analytically that most of the denominator factors have fixed sign in the s_{45} channel. For a few, we have statistical evidence based on 100K random phase-space points generated by sampling uniformly a parameterisation of the momenta in terms of energies and angles.

JHEP07(2024)073

We observe that, for a small fraction of phase-space points in the s_{45} channel, the straight line connecting them to $\vec{x}_0$ leaves the s_{45} channel. A similar structure of the physical phase space is discussed in ref. [30]. In such a case, one can either perform the analytic continuation, or choose a different starting point.

We use AMFlow to obtain the values of all MIs at $\vec{x}_0$ with, at least, 32-digit precision.[7] This gives an upper bound on the achievable precision in the numerical evaluation of the MIs using the results provided in this work. We expect this level of precision to be sufficient for the application in phenomenology at NNLO in QCD, based on the available experience with two-loop scattering amplitudes with kinematics of similar complexity. However, higher precision can be easily achieved, if needed, as evaluating the MIs in a single point with AMFlow does not represent a bottleneck for this computation. We provide the boundary values in the supplementary material [123].

For the topologies PB_A and PB_C, the canonical form of the DEs implies that the values at order ε^0 are rational, and can be determined up to the overall normalisation by imposing 'first-entry' conditions [131]. In other words, only logarithms of the following arguments can appear at order ε^1,

$$\{m_t^2\,,\ 2(d_{12}+m_t^2)\,,\ 2d_{23}\,,\ 2d_{34}\,,\ 2d_{45}\,,\ 2d_{15}\}\,, \tag{5.5}$$

and this gives linear constraints on the $\mathcal{O}(\varepsilon^0)$ boundary values. The allowed logarithm arguments can be read off from the graph polynomial $\mathcal{F}$. We then fix the overall normalisation by rationalising the values from AMFlow. Similarly, at order $\mathcal{O}(\varepsilon^1)$ we verify using the PSLQ algorithm [132] that the values are $\mathbb{Q}$-linear combinations of logarithms of the functions in eq. (5.5) evaluated at $\vec{x}_0$.

As for topology PB_B, although the DEs are not in canonical form, we still observe that the boundary values are rational at order ε^0, and linear combinations of the logarithms above at order ε^1. This follows from the fact that the 'problematic' MIs, namely those of the sector involving the nested square root ($\mathcal{I}_{\text{PB}_B,19}$ and $\mathcal{I}_{\text{PB}_B,20}$, see section 3.3) and those of the sector involving elliptic integrals ($\mathcal{I}_{\text{PB}_B,35}$, $\mathcal{I}_{\text{PB}_B,36}$ and $\mathcal{I}_{\text{PB}_B,37}$, see section 3.5), are non-zero only starting from order ε^4.

5.3 Checks

The rationality of the boundary values at order ε^0 and the first-entry conditions discussed in the previous subsection are already non-trivial checks of our results. In order to validate more robustly the numerical evaluation of the MIs, we compared the numerical values obtained by integrating the DEs with DiffExp starting from $\vec{x}_0$ against numerical evaluations performed with AMFlow at a number of points in the s_{45} channel. We found full agreement within the accuracy estimated by DiffExp and AMFlow. In particular, we perform this check at the following random point,

$$\vec{x}_1 = \left\{\frac{4602}{57095}, \frac{217}{8151}, -\frac{8513}{67193}, \frac{7}{22}, -\frac{14291}{77626}, \frac{1701}{90164}\right\}\,, \tag{5.6}$$

[7] We interfaced AMFlow to FiniteFlow and LiteRed for the required IBP reductions. The computation took from $\approx$ 12 hours for PB_A to $\approx$ 2 days for PB_B using 40 threads on an Intel(R) Xeon(R) Gold 5218 2.30 GHz CPU.

JHEP07(2024)073

which lies in the s_{45} channel on the other side of the spurious singularity $d_{12} + d_{15} + m_t^2 = 0$ with respect to the boundary point $\vec{x_0}$. This allows us to check the stability of the numerical evaluation when integrating the DEs over a path that crosses this spurious singularity. We provide the values of the master integrals at $\vec{x}_1$ as benchmarks in ancillary files [123].

5.4 Performance analysis

We finish this section by making some considerations regarding the performance of the numerical evaluation of the MIs. First of all, we want to clarify that our evaluation strategy is not optimised for phenomenological applications, and we therefore refrain from making absolute statements about the evaluation time. The latter in fact depends strongly on the segmentation of the path within the generalised power series expansion method [85, 101]. The number of segments, in turn, depends on the chosen endpoints of the path, and on the location of the nearest singularities. An evaluation strategy aimed at a large number of points should therefore minimise the number of segments in the evaluations by re-using iteratively the values obtained with previous evaluations (see e.g. ref. [35]). We leave this to future work.

Nonetheless, it is still interesting to compare the relative performance of the evaluation of the MIs of topologies PB_A, PB_C and PB_B, as the ε structure of the corresponding DEs is different. We recall that for topology PB_A and PB_C we have canonical DEs where ε is factorised, whereas the entries of the connection matrix of topology PB_B are degree-2 polynomials in ε. We can estimate the impact of the additional terms in ε for topology PB_B by comparing the evaluation time per segment between topologies for the same values of all parameters. We performed this analysis on a sample of 100 phase-space points in the s_{45} channel, amounting to ≈ 1.5 K segments starting from the boundary point $\vec{x}_0$, with a target accuracy of 10^{-16} in DiffExp. The results of this analysis are shown in figure 5.[8] The different ε structure for the DEs, together with the larger number of MIs, results in a higher evaluation time of PB_B with respect to PB_A and PB_C. Indeed, the average evaluation time per segment is ≈ 12 seconds for PB_A, ≈ 16 seconds for PB_C, and ≈ 58 seconds for PB_B.

A naive implementation in which each phase-space point is obtained by transporting from the boundary point the evaluation time would be rather slow, with the average time per point for PB_B of ≈ 15 minutes. For this reason a dynamic evaluation, in which each point is derived from the closest point in all previous evaluations, would be considerably more efficient (see e.g. refs. [35, 133, 134]). The algorithm to obtain the optimal route for the evaluation of a set of phase-space points remains for future work and will depend on the exact method used to combine real and virtual elements at NNLO. Such an algorithm would ensure a minimum number of segments is required to cover all phase-space points and so the average time per segment ≈ 1 min is a more relevant benchmark.

We finish this section with some comments. First, the data shown in figure 5 have to be intended as a qualitative analysis and not as a serious attempt of performing a statistical study of the evaluation time performance of the method. Furthermore, if we take into account the earlier analysis, bearing in mind that our evaluation strategy is not tailored for phenomenological applications, we find the current results to be promising. Finally, it would be interesting to compare the evaluation time of our solution with a possible generalised

[8] All the evaluations are performed on an Intel(R) Xeon(R) Gold 5218 2.30 GHz CPU.

JHEP07(2024)073

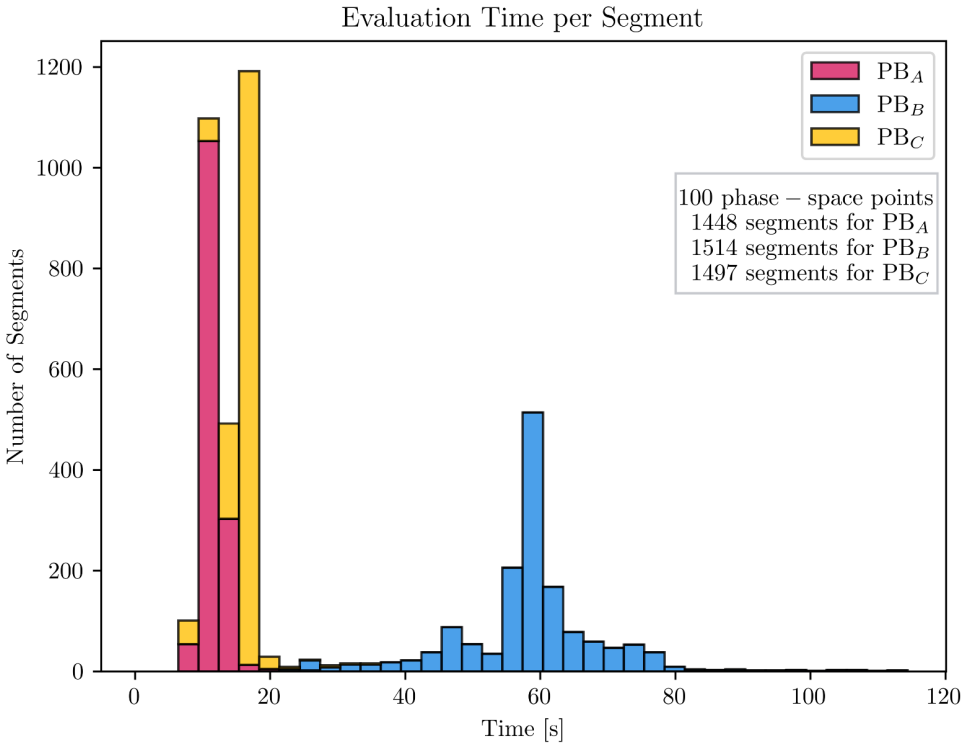

Figure 5. Histogram showing the distribution of the evaluation time per segment for topologies PB_A, PB_B and PB_C. Note that the number of segments depends on the singularity structure and is therefore different for each topology.

power series implementation for the case where the connection matrix contains elliptic kernels. Indeed, assuming to be able to build an integral basis in which the DEs are factorised also in the elliptic case, the resulting connection matrix will then depend on elliptic functions. Therefore, it will be interesting to weigh whether is the polynomial dependence on ε, or the presence of elliptic functions, to have the most significant impact on the numerical evaluation of the MIs.

6 Conclusion

In this work, we have presented compact differential equations for the master integrals of all integral topologies required to describe the production of a pair of top quarks in association with a jet at hadron colliders at NNLO in leading colour QCD. There were two new pentagon-box topologies to consider, PB_B (figure 1(b)) and PB_C (figure 1(c)). The latter followed a pattern similar to the one observed in ref. [19] for PB_A (figure 1(a)) and we obtain the DEs in the canonical form, i.e., such that the connection matrices are given by an overall factor of ε and $\mathbb{Q}$-linear combinations of logarithmic one-forms ($\mathrm{d}\log$'s). We showed that the former, PB_B, has new features that prevent it from having the same canonical form. While the one-loop topologies were previously studied and presented in ε-factorised form in ref. [19], we present them here for completeness in terms of $\mathrm{d}\log$'s.

JHEP07(2024)073

Topology PB_B displays two new features. First, the sector shown graphically in figure 2(b) involves a nested square root. Secondly, the sector in figure 2(a) involves elliptic integrals, which we identify as the periods of the elliptic curve in eq. (A.8). Obtaining canonical DEs in the presence of elliptic integrals is at the forefront of current research and the very notion of 'canonical' in such cases is still under debate. From a practical view point, even if such a generalised canonical form is achieved, the numerical evaluation of the solution remains challenging, and so an alternative route to efficient and stable numerical evaluation was taken. We obtain a compact representation of the differential equation in this case by making d log choices for all master integrals except those in the complicated sectors. For the problematic sectors, we find choices in which the differential equation is at most quadratic in ε. This form is compatible with rational reconstruction over finite fields using optimised IBP relations in the same fashion as the other topologies and with easily manageable computation times. By using a set of linearly independent d log and non-logarithmic one-forms we express the DEs in a compact form where the number of non-logarithmic structures is minimised.

We evaluate the master integrals numerically by solving the corresponding DEs by means of DiffExp [101], a Mathematica implementation of the method of generalised power series expansions [85]. We focus our analysis on the physical phase-space region relevant for $pp \to t\bar{t}$+jet, the s_{45} channel. We obtain numerical boundary values in this region with AMFlow [102], which implements the auxiliary mass flow method [104–106]. Interestingly, we observe that the master integrals related to the problematic features (that is, the nested square root and the elliptic curve) are non-zero only starting from order ε^4. We perform a number of checks that the numerical evaluation in the s_{45} channel is reliable and computationally feasible. We find that the quadratic ε-dependence of the DEs for topology PB_B results in an increase of the evaluation time of the method with respect to the ε-factorised DEs for topologies PB_A and PB_C. Nevertheless, given the level of optimisation of our solution, we find the performance analysis promising for future phenomenology applications.

There are still a number of issues to be addressed before the method can be applied in the context of amplitude computations. Proceeding without a representation of the integrals in terms of a basis of special functions order by order in ε means that the poles could not be removed analytically. The inability to perform an expansion in four dimensions may also mean that certain simplifications in the amplitude are not observed. Nevertheless, a strategy of performing the integration-by-parts reduction to master integrals numerically over a rationalised phase space with modular arithmetic appears to be achievable without major new technological developments. While combining this with an optimised strategy for the evaluation of the master integrals over the full phase space is left for future work, we remark that the application of the generalised series expansion method for phenomenological studies has been successful for other processes [133, 135–137]. It would also be interesting to continue the search for ε-factorised DEs for PB_B following the latest line of research in this area, which could potentially lead to even more efficient numerical evaluations. This would however require some substantial new developments in the available theoretical tools.

Our work paves the way to the analytic computation of the two-loop amplitudes for $pp \to t\bar{t}$+jet in the leading colour approximation, the main bottleneck towards obtaining predictions for this important process at NNLO in QCD.

JHEP07(2024)073

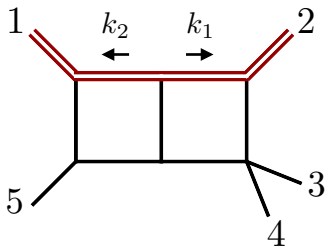

Figure 6. Four-point double-box super-sector of the elliptic sector in topology PB_B.

Acknowledgments

We are grateful to Heribertus Bayu Hartanto, Colomba Brancaccio, Ekta Chaubey and Christoph Dlapa for many enlightening discussions. We also thank Colomba Brancaccio and Xuhang Jiang for helpful comments on this paper. This project has received funding from the European Union's Horizon Europe research and innovation programme under the Marie Skłodowska-Curie grant agreement No. 101105486, and ERC Starting Grant No. 101040760 *FFHiggsTop*. This work has received funding from the Italian Ministry of Universities and Research through FARE grant R207777C4R. This research was supported in part by the Swiss National Science Foundation (SNF) under contract 200021_212729. SB has been partially supported by the Italian Ministry of Universities and Research (MUR) through grant PRIN 2022BCXSW9.

A Maximal-cut analysis of the elliptic sector

In this section, we analyse the maximal cut of the following scalar integral in the sector $321B$ of topology PB_B (see section 3.5 and figure 2(a)):

$$J = I^{(\mathrm{PB}_B),0,0,0}_{1,1,0,1,1,1,0,1}\,. \tag{A.1}$$

This is related to the basis integral $\mathcal{I}_{\mathrm{PB}_B,35}$ through eq. (3.31). The maximal cut is solution to the homogeneous DEs [117], and therefore contains precious information about the analytic structure of the full solution. We adopt the Baikov parametrisation [138, 139], and show that the maximal cut features the square root of a degree-4 polynomial. The latter defines an elliptic curve, whose periods (suitably normalised) are solutions to the Picard-Fuchs operator of $\mathcal{I}_{\mathrm{PB}_B,35}$ discussed in section 3.5.

Instead of starting from the Baikov parametrisation of the pentagon-box top sector, we view this sector as a sub-sector of the four-point double-box shown in figure 6. This allows us to get rid of two Baikov integration variables, corresponding to irreducible scalar products of the pentagon-box. Furthermore, we have one fewer integration variable by adopting a loop-by-loop Baikov parametrisation [139], starting from the k_2 loop.[9] Neglecting the overall

[9] Starting from the k_1 loop would lead to an equivalent result.

JHEP07(2024)073

kinematic-independent factors and the integration domain, our parametrisation is given by

$$J \propto [\det G(p_1,p_2,p_5)]^{\varepsilon} \int \frac{\mathrm{d}z_1\,\mathrm{d}z_2\,\mathrm{d}z_4\,\mathrm{d}z_5\,\mathrm{d}z_6\,\mathrm{d}z_8}{z_1\,z_2\,z_4\,z_5\,z_6\,z_8}\,\mathrm{d}z_7\,\mathrm{d}z_9 \times \\ [\det G(k_1,p_1,p_2,p_5)]^{-\frac{1}{2}-\varepsilon}\,[\det G(k_1,p_1,p_5)]^{\varepsilon}\,[\det G(k_2,k_1,p_1,p_5)]^{-\frac{1}{2}-\varepsilon}\,, \tag{A.2}$$

where we recall that G is the Gram matrix, i.e. $G_{ij}(v_1,\ldots,v_n) = v_i \cdot v_j$ for $i,j = 1,\ldots,n$, and the scalar products $k_i \cdot k_j$ and $k_i \cdot p_j$ are understood as written in terms of inverse propagators z_i. The maximal cut, namely the residue of the integrand at $z_i = 0$ for $i = 1,2,4,5,6,8$ in $d = 4$ dimensions is given by

$$\mathrm{MaxCut}\,[J]\,\big|_{\varepsilon=0} \propto \int \frac{\mathrm{d}z_7\,\mathrm{d}z_9}{\sqrt{f_1(z_9)\,f_2(z_9)\,f_3(z_7,z_9)}}\,, \tag{A.3}$$

where the f_i's are irreducible polynomials. In particular, $f_1(z_9) = z_9 + m_t^2$, $f_2(z_9)$ is a degree-2 polynomial in z_9, and $f_3(z_7,z_9)$ is a polynomial of degree 1 in z_9 and 2 in z_7. The dependence on the kinematic invariants is omitted.

We now wish to rewrite the integrand on the maximal cut as a linear combination of d log forms. The coefficients of the d log forms are called leading singularities. If this is possible, the integral — normalised so that its leading singularities are constant — is expected to satisfy canonical DEs [108]. For example, in the massless case (i.e., we set $m_t^2 = 0$ under the integral sign), we can write[10]

$$\mathrm{MaxCut}\,[J_{\mathrm{massless}}]\,\big|_{\varepsilon=0} \propto \frac{1}{d_{12}d_{15}} \int \mathrm{d}\log\left(z_7 - 2d_{15}\right)\,\mathrm{d}\log\left(1 - \frac{2d_{12}d_{15}}{z_9(d_{15}-d_{34})}\right)\,, \tag{A.4}$$

which indicates that $d_{12}d_{15}\,J_{\mathrm{massless}}$ — modulo sub-sector corrections — is a good candidate for a canonical basis. With a non-zero top-quark mass, however, only one differential form can be expressed as a d log,

$$\mathrm{MaxCut}\,[J]\,\big|_{\varepsilon=0} \propto \int \mathrm{d}\log\left[\alpha(z_7,z_9)\right]\,\frac{\mathrm{d}z_9}{\sqrt{\mathcal{P}(z_9)}}\,, \tag{A.5}$$

where $\alpha(z_7,z_9)$ is an irrelevant algebraic function, and $\mathcal{P}(z_9)$ is a degree-4 polynomial,

$$\mathcal{P}(z_9) = (z_9 + m_t^2)(z_9 - 3m_t^2)(\mathcal{P}_0 + \mathcal{P}_1\,z_9 + \mathcal{P}_2\,z_9^2)\,, \tag{A.6}$$

with

$$\begin{aligned}
\mathcal{P}_0 &= 4d_{12}^2d_{15}^2 + 4d_{12}d_{15}\,(d_{15}+d_{34})\,m_t^2 + \left(d_{15}^2 + 4d_{12}d_{34} + 2d_{15}d_{34} - 3d_{34}^2\right)m_t^4 + 2d_{34}m_t^6\,,\\
\mathcal{P}_1 &= 4d_{12}d_{15}\,(d_{34}-d_{15}) - 2\left(d_{15}^2 - 2d_{12}d_{34} + d_{34}^2\right)m_t^2\,,\\
\mathcal{P}_2 &= (d_{15}-d_{34})^2 - 2d_{34}m_t^2\,.
\end{aligned} \tag{A.7}$$

For generic values of the kinematic invariants, this degree-4 polynomial has four distinct roots, and thus defines an elliptic curve:

$$y^2 = \mathcal{P}(x)\,. \tag{A.8}$$

[10] We omit the exterior product between the differential forms to simplify the discussion.

JHEP07(2024)073

The differential form which cannot be expressed as a d log in eq. (A.5) is the holomorphic differential form of the first kind on this elliptic curve, which is one of the integration kernels defining the elliptic multiple polylogarithms [80] (see also ref. [84] for a similar example). In the massless limit ($m_t^2 = 0$), instead, two of the roots degenerate, so that $\mathcal{P}(z_9)$ becomes a perfect square and the elliptic curve reduces to a genus-zero surface. This is consistent with the fact that the massless pentagon-box integrals are of polylogarithmic type [27, 32].

The elliptic curve in eq. (A.8) contains useful information for putting the DEs in ε-factorised form, and is tightly connected to the Picard-Fuchs operator of the integral $\mathcal{I}_{\mathrm{PB}_B,35}$ discussed in section 3.5. In particular, we expect that the Feynman integral J normalised by a period of the elliptic curve in eq. (A.8) is a good candidate for a canonical integral [84]. While we leave this study for further work, we discuss here the connection with the Picard-Fuchs operator.

For this purpose, we must first spell out the periods of the elliptic curve. The four roots are given by[11]

$$\begin{aligned} e_1 &= -m_t^2\,, \\ e_2 &= \frac{2d_{12}d_{15}(d_{34}-d_{15}) - (d_{15}^2 + d_{34}^2 - 2d_{12}d_{34})m_t^2 + d_{34}\sqrt{\delta}}{\det G(p_2, p_1+p_5)}\,, \\ e_3 &= e_2\big|_{\sqrt{\delta}\to-\sqrt{\delta}}\,, \\ e_4 &= 3m_t^2\,, \end{aligned} \tag{A.9}$$

where

$$\delta = -4\, m_t^2 \det G(p_1, p_2, p_5)\,. \tag{A.10}$$

The periods can then be chosen as [125]

$$\psi_1 = \frac{4\,\mathrm{K}(\kappa^2)}{\sqrt{(e_3-e_1)(e_4-e_2)}}\,, \qquad \psi_2 = \frac{4\,\mathrm{i}\,\mathrm{K}(1-\kappa^2)}{\sqrt{(e_3-e_1)(e_4-e_2)}}\,, \tag{A.11}$$

where $\mathrm{K}(x)$ is the elliptic integral of the first kind, and κ is the modulus of the elliptic curve,

$$\kappa^2 = \frac{(e_3-e_2)(e_4-e_1)}{(e_3-e_1)(e_4-e_2)}\,. \tag{A.12}$$

Note that e_2 and e_3 involve a square root, and thus the periods feature another nested square root, in addition to the one discussed in section 3.3. We find that — with a suitable algebraic normalisation — the periods ψ_i are solutions to the Picard-Fuchs operator L_{35} of the Feynman integral $\mathcal{I}_{\mathrm{PB}_B,35}$ (modulo sub-sectors and ε-corrections). Explicitly, we have that

$$L_{35}\left[\frac{d_{15}(d_{12}+m_t^2)\,\psi_i}{\sqrt{(d_{15}-d_{34})^2 - 2d_{34}m_t^2}}\right] = 0\,, \tag{A.13}$$

for $i = 1, 2$, where the terms in the square brackets are understood as evaluated on the univariate phase-space slice used to derive L_{35}. The rational factors multiplying the periods

[11] In the s_{45} channel we have that $e_1 < 0$, $e_4 > 0$, $\delta < 0$, while the real parts of e_2 and e_3 do not have fixed sign.

JHEP07(2024)073

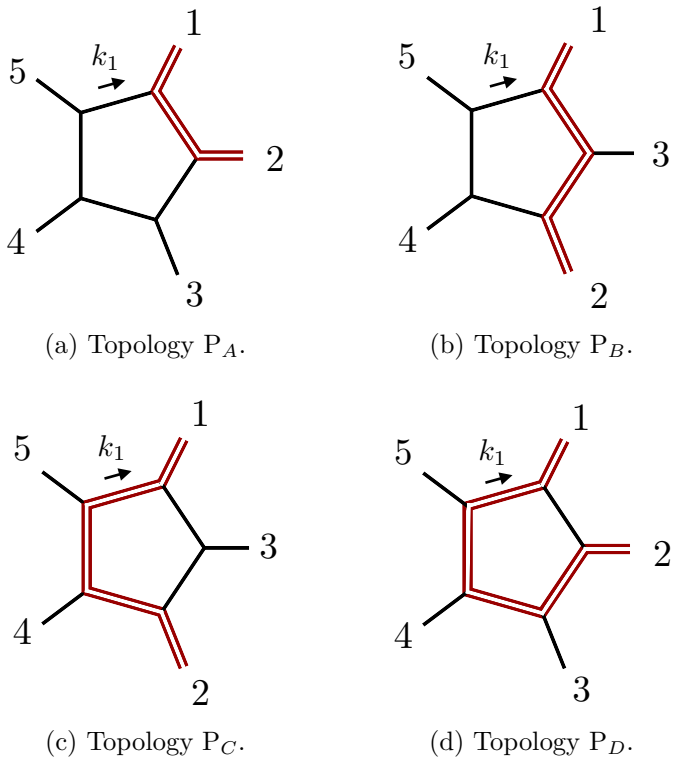

(a) Topology P_A. (b) Topology P_B.

(c) Topology P_C. (d) Topology P_D.

Figure 7. Graphical representation of the four one-loop pentagon topologies.

follow from the chosen normalisation of $\mathcal{I}_{\mathrm{PB}_B,35}$ (see eq. (3.31)), while the square root is the coefficient of the degree-4 monomial in the polynomial $\mathcal{P}$ defining the elliptic curve. With this, we have established that the elliptic integrals found in the solutions to the Picard-Fuchs operator L_{35} in section 3.5 and thus in the homogeneous solution to the DEs are associated with the elliptic curve given in eq. (A.8).

B All one-loop pentagon integrals

We update the representation of the differential equations for all one-loop pentagon integrals contributing to $pp \to t\bar{t}$+jet previously considered in reference [19]. We present them in 'd log' form using an alphabet which shares as much in common with the two-loop planar integrals as possible. For completeness we include here the definitions of the integral families which are shown graphically in figure 7. The integrals of the pentagon topology $F \in \{\mathrm{P}_A, \mathrm{P}_B, \mathrm{P}_C, \mathrm{P}_D\}$ have the form

$$I^{(F)}_{a_1,a_2,a_3,a_4,a_5} = \int \mathcal{D}^d k_1 \, \frac{1}{D^{a_1}_{F,1} \cdots D^{a_5}_{F,5}} \,, \tag{B.1}$$

where we recall that the integration measure $\mathcal{D}^d k_1$ is defined in eq. (2.2). The inverse propagators $D_{F,i}$ are defined in table 3.

JHEP07(2024)073

	P_A	P_B	P_C	P_D
$D_{F,1}$	k_1^2	k_1^2	$k_1^2 - m_t^2$	$k_1^2 - m_t^2$
$D_{F,2}$	$(k_1 - p_1)^2 - m_t^2$	$(k_1 - p_1)^2 - m_t^2$	$(k_1 - p_1)^2$	$(k_1 - p_1)^2$
$D_{F,3}$	$(k_1 - p_1 - p_2)^2$	$(k_1 - p_1 - p_3)^2 - m_t^2$	$(k_1 - p_1 - p_3)^2$	$(k_1 - p_1 - p_2)^2 - m_t^2$
$D_{F,4}$	$(k_1 + p_4 + p_5)^2$	$(k_1 + p_4 + p_5)^2$	$(k_1 + p_4 + p_5)^2 - m_t^2$	$(k_1 + p_4 + p_5)^2 - m_t^2$
$D_{F,5}$	$(k_1 + p_5)^2$	$(k_1 + p_5)^2$	$(k_1 + p_5)^2 - m_t^2$	$(k_1 + p_5)^2 - m_t^2$

Table 3. Inverse propagators $D_{F,i}$ of the pentagon topologies shown in figure 7.

C Description of the ancillary files

The ancillary files can be downloaded from ref. [123]. The symbols in the files are given in the notation of the article as follows:

$$\begin{aligned}
\texttt{eps} &= \varepsilon\,, & \texttt{W[i]} &= W_i\,,\\
\texttt{dij} &= d_{ij}\,, & \texttt{j[F,a1,...,a5]} &= I^{(F)}_{a_1,\ldots,a_5}\,,\\
\texttt{mt2} &= m_t^2\,, & \texttt{j[F,a1,...,a11]} &= I^{(F),-a_9,-a_{10},-a_{11}}_{a_1,\ldots,a_8}\,,\\
\texttt{s[i,j]} &= s_{ij}\,, & \texttt{dlog[W[i]]} &= \mathrm{d}\log\left(W_i\right)\,,\\
\texttt{s[i]} &= p_i^2\,, & \texttt{of[i]} &= \omega_i\,,\\
\texttt{pi} &= p_i\,, & \texttt{GramDet[P1,...,Pn]} &= \det G(P_1,\ldots,P_n)\,,\\
\texttt{ki} &= k_i\,, & \texttt{trp[i1,...,in]} &= \mathrm{tr}_+\left[\not{p}_{i_1}\ldots\not{p}_{i_n}\right]\,,\\
\texttt{p[i,j]} &= p_{ij}\,, & \texttt{trm[i1,...,in]} &= \mathrm{tr}_-\left[\not{p}_{i_1}\ldots\not{p}_{i_n}\right]\,,\\
\texttt{spAB[i,...,j]} &= \langle i|\ldots|j]\,, & \texttt{sqrtratio[a,b]} &= \frac{a+b}{a-b}\,.
\end{aligned}$$

The following files give global definitions of the square roots, the alphabet letters and the physical scattering region under consideration.

- `square_roots.m` — definition of the square roots in the format

  $$\texttt{\{ ..., S -> Sqrt[expr] , ...\}}\,,$$

  where `S` is the square-root label,

  $$\begin{aligned}
  &\texttt{tr5} = \mathrm{tr}_5, \quad \texttt{beta12} = \beta_{12}, \quad \texttt{beta34} = \beta_{34}, \quad \texttt{beta45} = \beta_{45}, \quad \texttt{Delta31} = \Delta_{3,1},\\
  &\texttt{Delta32} = \Delta_{3,2}, \quad \texttt{Delta33} = \Delta_{3,3}, \quad \texttt{Delta34} = \Delta_{3,4}, \quad \texttt{Lambda1} = \Lambda_1, \quad \texttt{Lambda2} = \Lambda_2,\\
  &\texttt{Lambda3} = \Lambda_3, \quad \texttt{Lambda4} = \Lambda_4, \quad \texttt{Lambda5} = \Lambda_5, \quad \texttt{Lambda6} = \Lambda_6,
  \end{aligned}$$

  and `expr` is a rational function of the invariants $\vec{x}$. See section 2 for a representation in terms of Gram and Cayley determinants.

- `alphabet.m` — definition of the alphabet letters W_i in the format

  $$\texttt{\{..., W[i] -> expr, ...\}}\,,$$

JHEP07(2024)073

where `expr` is given in terms of invariants $\vec{x}$, s_{ij} variables, Gram determinants, spinor-helicity chains, and gamma-matrix traces.

- `alphabet_dij.m` — definition of the alphabet letters `W[i]` in the same format as in `alphabet.m`, but with `expr` given in terms of invariants $\vec{x}$ and square roots.

- `alphabet_charges.m` — charges of the letters in the format

  ```
  {..., C -> {W[i1],W[i2],...},...},
  ```

  meaning that the letters $\{W_{i_1}, W_{i_2}, \ldots\}$ are odd with respect to the square-root monomial `C`. The letters with `C` $= 1$ are rational, and thus even with respect to all square roots. See the introduction of section 3 for the notion of charge.

- `s45-channel.m` — the inequalities in the d_{ij} variables which define the s_{45} channel (see section 5.1).

For each integral topology `<fam>` studied in this work there is a folder with the same name containing the definition of the propagators and of the integral basis, the differential equations, and the boundary values. The integral topologies are denoted by

$$\texttt{PttjA} = \mathrm{P}_A\,, \qquad \texttt{PttjB} = \mathrm{P}_B\,, \qquad \texttt{PttjC} = \mathrm{P}_C\,, \qquad \texttt{PttjD} = \mathrm{P}_D\,,$$
$$\texttt{PBttjA} = \mathrm{PB}_A\,, \qquad \texttt{PBttjB} = \mathrm{PB}_B\,, \qquad \texttt{PBttjC} = \mathrm{PB}_C\,.$$

The folder of the family `<fam>` contains the following files.

- `<fam>_propagators.m` — the inverse propagators $D_{F,i}$.

- `<fam>_basis_definitions.m` — the definition of the (square-root free) integral basis in the format

  ```
  {..., mi[<fam>,i] -> expr, ...},
  ```

  where `mi[<fam>,i]` denotes the i-th master integral of the topology `<fam>`, and `expr` is a linear combination of scalar integrals with coefficients given by rational functions of the invariants $\vec{x}$ and ε.

- `<fam>_basis_norm.m` — the square-root normalisations that should be applied in addition to the basis integrals. More explicitly, the i-th master integral in `<fam>_basis_definitions.m` has to be multiplied by the i-th entry of `<fam>_basis_norm.m`. The separation between rational expressions and square roots is motivated in section 3.

- `<fam>_de_dlogs.m` (or `PBttjB_de_one-forms.m` where the d log-representation is not possible) — the connection matrices of the differential equations for the master integrals expressed in terms of d log's and, for PB_B, one-forms ω_i.

JHEP07(2024)073

- `<fam>_boundary_values_s45.m` — phase-space point and numerical values of the master integrals in the s_{45} scattering region with at least 32-digit precision. The format is `{X,values}`. The first entry, `X`, gives the boundary point $\vec{x}_0$ defined in eq. (5.4), in the format

  ```
  <|d12->2, d23->1, d34->-1, d45->5, d15 ->-2, mt2->1|>.
  ```

  The second entry, `values`, is a $n_{\text{MI}} \times 5$ array, where n_{MI} is the number of master integrals of the family, and 5 is the number of orders in ε (from ε^0 to ε^4). The entry (i, j) of `values` gives the value of the $\mathcal{O}\left(\varepsilon^{j-1}\right)$ coefficient of the i-th master integral.

The folder for topology PB_B contains two additional files, due to the fact that the differential equations cannot be expressed in terms of d log's only.

- `PBttjB_one-forms_definitions.m` — definition of the one-forms ω_i in the format

  ```
  {..., of[i] -> {r1,r2,...,r6}, ...},
  ```

  meaning that

  $$\omega_i(\vec{x}) = \sum_{j=1}^{6} r_j(\vec{x})\, \mathrm{d}x_j \,,$$

  where $r_j =$ `rj` are functions of the invariants $\vec{x}$ and of the square roots.

- `PBttjB_one-forms_charges.m` — charges of the one-forms in the format

  ```
  {...,C -> {of[i1],of[i2],...},...},
  ```

  meaning that the one-forms $\{\omega_{i_1}, \omega_{i_2}, \ldots\}$ are odd with respect to the square-root monomial `C`. The one-forms with `C` $= 1$ are rational, and thus even with respect to all square roots.

The folder `benchmarks/` contains benchmark values of all basis integrals.

- `point_x1_s45.m` — phase-space point $\vec{x}_1$ in the s_{45} channel defined in eq. (5.6), in the format

  ```
  {d12->#val, d23->#val, d34->#val, d45->#val, d15 ->#val, mt2->#val},
  ```
  (C.1)

  where `#val` denotes a numerical value.

- `<fam>_values_x1.m` — values of the basis integrals of family `<fam>` at the phase-space point $\vec{x}_1$ with at least 32-digit precision. The format is the same as in `<fam>_boundary_values_s45.m`.

JHEP07(2024)073

A MATHEMATICA script, `DiffExp_run.wl`, is provided to evaluate numerically the basis integrals through DIFFEXP [101]. The path to `DiffExp.m` has to be specified through the variable `PathToDiffExp`. The script may be used via the command line as

```
math -script DiffExp_run.wl [-family <fam>] [-target <file>] [-storepiecewise]
```

The file indicated to be the target phase-space point is expected in the format shown in eq. (C.1). If the option `-storepiecewise` is given, the script also stores the analytic expression of the generalised power series solution to the differential equations. Otherwise, only the numerical values of the basis integrals at the target point are saved, in the `benchmarks/` folder. The integration of the differential equations occurs along a straight path connecting the target point to the boundary point $\vec{x}_0$ in eq. (5.4). If the path leaves the s_{45} channel, the evaluation is aborted. This may occur even if the target point is in the s_{45} channel. In such a case, one should either choose a different starting point for the integration path, or study the analytic continuation from the s_{45} channel to the region of interest. The latter is instead mandatory if the target point is outside of the s_{45} channel. The accuracy goal is hard-coded to 16 digits. If the target point is $\vec{x}_1$, the evaluations are compared against the provided benchmark values.

References

[1] CMS collaboration, *Measurement of differential cross sections for top quark pair production using the lepton+jets final state in proton-proton collisions at 13 TeV*, *Phys. Rev. D* **95** (2017) 092001 [arXiv:1610.04191] [INSPIRE].

[2] ATLAS collaboration, *Measurements of differential cross sections of top quark pair production in association with jets in pp collisions at $\sqrt{s} = 13$ TeV using the ATLAS detector*, *JHEP* **10** (2018) 159 [arXiv:1802.06572] [INSPIRE].

[3] CMS collaboration, *Measurement of the cross section for $t\bar{t}$ production with additional jets and b jets in pp collisions at $\sqrt{s} = 13$ TeV*, *JHEP* **07** (2020) 125 [arXiv:2003.06467] [INSPIRE].

[4] CMS collaboration, *Differential cross section measurements for the production of top quark pairs and of additional jets using dilepton events from pp collisions at $\sqrt{s} = 13$ TeV*, arXiv:2402.08486 [INSPIRE].

[5] S. Alioli et al., *A new observable to measure the top-quark mass at hadron colliders*, *Eur. Phys. J. C* **73** (2013) 2438 [arXiv:1303.6415] [INSPIRE].

[6] G. Bevilacqua et al., *Top quark mass studies with $t\bar{t}j$ at the LHC*, *JHEP* **03** (2018) 169 [arXiv:1710.07515] [INSPIRE].

[7] S. Alioli et al., *Phenomenology of $t\bar{t}j$ + X production at the LHC*, *JHEP* **05** (2022) 146 [arXiv:2202.07975] [INSPIRE].

[8] ATLAS collaboration, *Measurement of the top-quark mass in $t\bar{t}+1$-jet events collected with the ATLAS detector in pp collisions at $\sqrt{s} = 8$ TeV*, *JHEP* **11** (2019) 150 [arXiv:1905.02302] [INSPIRE].

JHEP07(2024)073

[9] J.L. Bourjaily et al., *Functions Beyond Multiple Polylogarithms for Precision Collider Physics*, in the proceedings of the *Snowmass 2021*, Seattle, U.S.A., July 17–26 (2022) [arXiv:2203.07088] [INSPIRE].

[10] S. Dittmaier, P. Uwer and S. Weinzierl, *NLO QCD corrections to $t\bar{t}$ + jet production at hadron colliders*, *Phys. Rev. Lett.* **98** (2007) 262002 [hep-ph/0703120] [INSPIRE].

[11] S. Dittmaier, P. Uwer and S. Weinzierl, *Hadronic top-quark pair production in association with a hard jet at next-to-leading order QCD: Phenomenological studies for the Tevatron and the LHC*, *Eur. Phys. J. C* **59** (2009) 625 [arXiv:0810.0452] [INSPIRE].

[12] K. Melnikov and M. Schulze, *NLO QCD corrections to top quark pair production in association with one hard jet at hadron colliders*, *Nucl. Phys. B* **840** (2010) 129 [arXiv:1004.3284] [INSPIRE].

[13] S. Alioli, S.-O. Moch and P. Uwer, *Hadronic top-quark pair-production with one jet and parton showering*, *JHEP* **01** (2012) 137 [arXiv:1110.5251] [INSPIRE].

[14] M. Czakon, H.B. Hartanto, M. Kraus and M. Worek, *Matching the Nagy-Soper parton shower at next-to-leading order*, *JHEP* **06** (2015) 033 [arXiv:1502.00925] [INSPIRE].

[15] G. Bevilacqua, H.B. Hartanto, M. Kraus and M. Worek, *Top Quark Pair Production in Association with a Jet with Next-to-Leading-Order QCD Off-Shell Effects at the Large Hadron Collider*, *Phys. Rev. Lett.* **116** (2016) 052003 [arXiv:1509.09242] [INSPIRE].

[16] G. Bevilacqua, H.B. Hartanto, M. Kraus and M. Worek, *Off-shell Top Quarks with One Jet at the LHC: A comprehensive analysis at NLO QCD*, *JHEP* **11** (2016) 098 [arXiv:1609.01659] [INSPIRE].

[17] C. Gütschow, J.M. Lindert and M. Schönherr, *Multi-jet merged top-pair production including electroweak corrections*, *Eur. Phys. J. C* **78** (2018) 317 [arXiv:1803.00950] [INSPIRE].

[18] J.M. Campbell et al., *Event Generators for High-Energy Physics Experiments*, *SciPost Phys.* **16** (2024) 130 [arXiv:2203.11110] [INSPIRE].

[19] S. Badger et al., *One-loop QCD helicity amplitudes for $pp \to t\bar{t}j$ to $O(\varepsilon^2)$*, *JHEP* **06** (2022) 066 [arXiv:2201.12188] [INSPIRE].

[20] S. Badger, M. Becchetti, E. Chaubey and R. Marzucca, *Two-loop master integrals for a planar topology contributing to $pp \to t\bar{t}j$*, *JHEP* **01** (2023) 156 [arXiv:2210.17477] [INSPIRE].

[21] A.V. Kotikov, *Differential equations method: New technique for massive Feynman diagrams calculation*, *Phys. Lett. B* **254** (1991) 158 [INSPIRE].

[22] E. Remiddi, *Differential equations for Feynman graph amplitudes*, *Nuovo Cim. A* **110** (1997) 1435 [hep-th/9711188] [INSPIRE].

[23] J.M. Henn, *Multiloop integrals in dimensional regularization made simple*, *Phys. Rev. Lett.* **110** (2013) 251601 [arXiv:1304.1806] [INSPIRE].

[24] A. von Manteuffel and R.M. Schabinger, *A novel approach to integration by parts reduction*, *Phys. Lett. B* **744** (2015) 101 [arXiv:1406.4513] [INSPIRE].

[25] T. Peraro, *Scattering amplitudes over finite fields and multivariate functional reconstruction*, *JHEP* **12** (2016) 030 [arXiv:1608.01902] [INSPIRE].

[26] T. Peraro, *FiniteFlow: multivariate functional reconstruction using finite fields and dataflow graphs*, *JHEP* **07** (2019) 031 [arXiv:1905.08019] [INSPIRE].

JHEP07(2024)073

[27] T. Gehrmann, J.M. Henn and N.A. Lo Presti, *Analytic form of the two-loop planar five-gluon all-plus-helicity amplitude in QCD*, *Phys. Rev. Lett.* **116** (2016) 062001 [*Erratum ibid.* **116** (2016) 189903] [arXiv:1511.05409] [INSPIRE].

[28] T. Gehrmann, J.M. Henn and N.A. Lo Presti, *Pentagon functions for massless planar scattering amplitudes*, *JHEP* **10** (2018) 103 [arXiv:1807.09812] [INSPIRE].

[29] D. Chicherin and V. Sotnikov, *Pentagon Functions for Scattering of Five Massless Particles*, *JHEP* **12** (2020) 167 [arXiv:2009.07803] [INSPIRE].

[30] D. Chicherin, V. Sotnikov and S. Zoia, *Pentagon functions for one-mass planar scattering amplitudes*, *JHEP* **01** (2022) 096 [arXiv:2110.10111] [INSPIRE].

[31] S. Abreu et al., *All Two-Loop Feynman Integrals for Five-Point One-Mass Scattering*, *Phys. Rev. Lett.* **132** (2024) 141601 [arXiv:2306.15431] [INSPIRE].

[32] C.G. Papadopoulos, D. Tommasini and C. Wever, *The Pentabox Master Integrals with the Simplified Differential Equations approach*, *JHEP* **04** (2016) 078 [arXiv:1511.09404] [INSPIRE].

[33] S. Abreu et al., *The two-loop five-point amplitude in $\mathcal{N} = 4$ super-Yang-Mills theory*, *Phys. Rev. Lett.* **122** (2019) 121603 [arXiv:1812.08941] [INSPIRE].

[34] D. Chicherin et al., *All Master Integrals for Three-Jet Production at Next-to-Next-to-Leading Order*, *Phys. Rev. Lett.* **123** (2019) 041603 [arXiv:1812.11160] [INSPIRE].

[35] S. Abreu et al., *Two-Loop Integrals for Planar Five-Point One-Mass Processes*, *JHEP* **11** (2020) 117 [arXiv:2005.04195] [INSPIRE].

[36] D.D. Canko, C.G. Papadopoulos and N. Syrrakos, *Analytic representation of all planar two-loop five-point Master Integrals with one off-shell leg*, *JHEP* **01** (2021) 199 [arXiv:2009.13917] [INSPIRE].

[37] S. Abreu, H. Ita, B. Page and W. Tschernow, *Two-loop hexa-box integrals for non-planar five-point one-mass processes*, *JHEP* **03** (2022) 182 [arXiv:2107.14180] [INSPIRE].

[38] S. Badger, C. Brønnum-Hansen, H.B. Hartanto and T. Peraro, *Analytic helicity amplitudes for two-loop five-gluon scattering: the single-minus case*, *JHEP* **01** (2019) 186 [arXiv:1811.11699] [INSPIRE].

[39] S. Abreu et al., *Planar Two-Loop Five-Parton Amplitudes from Numerical Unitarity*, *JHEP* **11** (2018) 116 [arXiv:1809.09067] [INSPIRE].

[40] D. Chicherin et al., *Analytic result for a two-loop five-particle amplitude*, *Phys. Rev. Lett.* **122** (2019) 121602 [arXiv:1812.11057] [INSPIRE].

[41] S. Abreu et al., *Analytic Form of Planar Two-Loop Five-Gluon Scattering Amplitudes in QCD*, *Phys. Rev. Lett.* **122** (2019) 082002 [arXiv:1812.04586] [INSPIRE].

[42] S. Badger et al., *Analytic form of the full two-loop five-gluon all-plus helicity amplitude*, *Phys. Rev. Lett.* **123** (2019) 071601 [arXiv:1905.03733] [INSPIRE].

[43] S. Abreu et al., *Analytic Form of the Planar Two-Loop Five-Parton Scattering Amplitudes in QCD*, *JHEP* **05** (2019) 084 [arXiv:1904.00945] [INSPIRE].

[44] H.B. Hartanto, S. Badger, C. Brønnum-Hansen and T. Peraro, *A numerical evaluation of planar two-loop helicity amplitudes for a W-boson plus four partons*, *JHEP* **09** (2019) 119 [arXiv:1906.11862] [INSPIRE].

[45] D. Chicherin et al., *The two-loop five-particle amplitude in $\mathcal{N} = 8$ supergravity*, *JHEP* **03** (2019) 115 [arXiv:1901.05932] [INSPIRE].

JHEP07(2024)073

[46] S. Abreu, B. Page, E. Pascual and V. Sotnikov, *Leading-Color Two-Loop QCD Corrections for Three-Photon Production at Hadron Colliders*, *JHEP* **01** (2021) 078 [arXiv:2010.15834] [INSPIRE].

[47] H.A. Chawdhry, M. Czakon, A. Mitov and R. Poncelet, *Two-loop leading-color helicity amplitudes for three-photon production at the LHC*, *JHEP* **06** (2021) 150 [arXiv:2012.13553] [INSPIRE].

[48] S. Caron-Huot et al., *Multi-Regge Limit of the Two-Loop Five-Point Amplitudes in $\mathcal{N} = 4$ Super Yang-Mills and $\mathcal{N} = 8$ Supergravity*, *JHEP* **10** (2020) 188 [arXiv:2003.03120] [INSPIRE].

[49] S. Abreu et al., *Leading-color two-loop amplitudes for four partons and a W boson in QCD*, *JHEP* **04** (2022) 042 [arXiv:2110.07541] [INSPIRE].

[50] S. Badger, H.B. Hartanto, J. Kryś and S. Zoia, *Two-loop leading-colour QCD helicity amplitudes for Higgs boson production in association with a bottom-quark pair at the LHC*, *JHEP* **11** (2021) 012 [arXiv:2107.14733] [INSPIRE].

[51] B. Agarwal, F. Buccioni, A. von Manteuffel and L. Tancredi, *Two-loop leading colour QCD corrections to $q\bar{q} \to \gamma\gamma g$ and $qg \to \gamma\gamma q$*, *JHEP* **04** (2021) 201 [arXiv:2102.01820] [INSPIRE].

[52] S. Badger et al., *Virtual QCD corrections to gluon-initiated diphoton plus jet production at hadron colliders*, *JHEP* **11** (2021) 083 [arXiv:2106.08664] [INSPIRE].

[53] H.A. Chawdhry, M. Czakon, A. Mitov and R. Poncelet, *Two-loop leading-colour QCD helicity amplitudes for two-photon plus jet production at the LHC*, *JHEP* **07** (2021) 164 [arXiv:2103.04319] [INSPIRE].

[54] S. Badger, H.B. Hartanto and S. Zoia, *Two-Loop QCD Corrections to $Wb\bar{b}$ Production at Hadron Colliders*, *Phys. Rev. Lett.* **127** (2021) 012001 [arXiv:2102.02516] [INSPIRE].

[55] S. Abreu et al., *Leading-color two-loop QCD corrections for three-jet production at hadron colliders*, *JHEP* **07** (2021) 095 [arXiv:2102.13609] [INSPIRE].

[56] B. Agarwal, F. Buccioni, A. von Manteuffel and L. Tancredi, *Two-Loop Helicity Amplitudes for Diphoton Plus Jet Production in Full Color*, *Phys. Rev. Lett.* **127** (2021) 262001 [arXiv:2105.04585] [INSPIRE].

[57] S. Badger, H.B. Hartanto, J. Kryś and S. Zoia, *Two-loop leading colour helicity amplitudes for $W^{\pm}\gamma$ + j production at the LHC*, *JHEP* **05** (2022) 035 [arXiv:2201.04075] [INSPIRE].

[58] H.B. Hartanto, R. Poncelet, A. Popescu and S. Zoia, *NNLO QCD corrections to $Wb\bar{b}$ production at the LHC*, *Phys. Rev. D* **106** (2022) 074016 [arXiv:2205.01687] [INSPIRE].

[59] S. Abreu et al., *Two-loop QCD corrections for three-photon production at hadron colliders*, *SciPost Phys.* **15** (2023) 157 [arXiv:2305.17056] [INSPIRE].

[60] G. De Laurentis, H. Ita and V. Sotnikov, *Double-virtual NNLO QCD corrections for five-parton scattering. II. The quark channels*, *Phys. Rev. D* **109** (2024) 094024 [arXiv:2311.18752] [INSPIRE].

[61] S. Badger et al., *Isolated photon production in association with a jet pair through next-to-next-to-leading order in QCD*, *JHEP* **10** (2023) 071 [arXiv:2304.06682] [INSPIRE].

[62] G. De Laurentis, H. Ita, M. Klinkert and V. Sotnikov, *Double-virtual NNLO QCD corrections for five-parton scattering. I. The gluon channel*, *Phys. Rev. D* **109** (2024) 094023 [arXiv:2311.10086] [INSPIRE].

[63] B. Agarwal et al., *Five-parton scattering in QCD at two loops*, *Phys. Rev. D* **109** (2024) 094025 [arXiv:2311.09870] [INSPIRE].

JHEP07(2024)073

[64] H.A. Chawdhry, M.L. Czakon, A. Mitov and R. Poncelet, *NNLO QCD corrections to three-photon production at the LHC*, *JHEP* **02** (2020) 057 [arXiv:1911.00479] [INSPIRE].

[65] S. Kallweit, V. Sotnikov and M. Wiesemann, *Triphoton production at hadron colliders in NNLO QCD*, *Phys. Lett. B* **812** (2021) 136013 [arXiv:2010.04681] [INSPIRE].

[66] H.A. Chawdhry, M. Czakon, A. Mitov and R. Poncelet, *NNLO QCD corrections to diphoton production with an additional jet at the LHC*, *JHEP* **09** (2021) 093 [arXiv:2105.06940] [INSPIRE].

[67] S. Badger, T. Gehrmann, M. Marcoli and R. Moodie, *Next-to-leading order QCD corrections to diphoton-plus-jet production through gluon fusion at the LHC*, *Phys. Lett. B* **824** (2022) 136802 [arXiv:2109.12003] [INSPIRE].

[68] X. Chen et al., *Automation of antenna subtraction in colour space: gluonic processes*, *JHEP* **10** (2022) 099 [arXiv:2203.13531] [INSPIRE].

[69] L. Buonocore et al., *Associated production of a W boson and massive bottom quarks at next-to-next-to-leading order in QCD*, *Phys. Rev. D* **107** (2023) 074032 [arXiv:2212.04954] [INSPIRE].

[70] H.B. Hartanto, R. Poncelet, A. Popescu and S. Zoia, *Flavour anti-k_T algorithm applied to $Wb\bar{b}$ production at the LHC*, arXiv:2209.03280 [INSPIRE].

[71] J. Mazzitelli, V. Sotnikov and M. Wiesemann, *Next-to-next-to-leading order event generation for Z-boson production in association with a bottom-quark pair*, arXiv:2404.08598 [INSPIRE].

[72] J. Henn, T. Peraro, Y. Xu and Y. Zhang, *A first look at the function space for planar two-loop six-particle Feynman integrals*, *JHEP* **03** (2022) 056 [arXiv:2112.10605] [INSPIRE].

[73] J.M. Henn et al., *A computation of two-loop six-point Feynman integrals in dimensional regularization*, arXiv:2403.19742 [INSPIRE].

[74] F. Febres Cordero et al., *Two-Loop Master Integrals for Leading-Color $pp \to t\bar{t}H$ Amplitudes with a Light-Quark Loop*, arXiv:2312.08131 [INSPIRE].

[75] F. Buccioni, P.A. Kreer, X. Liu and L. Tancredi, *One loop QCD corrections to $gg \to t\bar{t}H$ at $\mathcal{O}(\epsilon^2)$*, *JHEP* **03** (2024) 093 [arXiv:2312.10015] [INSPIRE].

[76] B. Agarwal et al., *Two-loop amplitudes for $t\bar{t}H$ production: the quark-initiated N_f-part*, *JHEP* **05** (2024) 013 [arXiv:2402.03301] [INSPIRE].

[77] S. Catani et al., *Higgs Boson Production in Association with a Top-Antitop Quark Pair in Next-to-Next-to-Leading Order QCD*, *Phys. Rev. Lett.* **130** (2023) 111902 [arXiv:2210.07846] [INSPIRE].

[78] G. Wang, T. Xia, L.L. Yang and X. Ye, *Two-loop QCD amplitudes for $t\bar{t}H$ production from boosted limit*, arXiv:2402.00431 [INSPIRE].

[79] J. Broedel, C. Duhr, F. Dulat and L. Tancredi, *Elliptic polylogarithms and iterated integrals on elliptic curves. Part I: general formalism*, *JHEP* **05** (2018) 093 [arXiv:1712.07089] [INSPIRE].

[80] J. Broedel et al., *Elliptic Feynman integrals and pure functions*, *JHEP* **01** (2019) 023 [arXiv:1809.10698] [INSPIRE].

[81] J. Broedel et al., *Elliptic symbol calculus: from elliptic polylogarithms to iterated integrals of Eisenstein series*, *JHEP* **08** (2018) 014 [arXiv:1803.10256] [INSPIRE].

[82] J. Broedel et al., *Elliptic polylogarithms and Feynman parameter integrals*, *JHEP* **05** (2019) 120 [arXiv:1902.09971] [INSPIRE].

JHEP07(2024)073

[83] H. Frellesvig and S. Weinzierl, *On ε-factorised bases and pure Feynman integrals*, *SciPost Phys.* **16** (2024) 150 [arXiv:2301.02264] [INSPIRE].

[84] L. Görges, C. Nega, L. Tancredi and F.J. Wagner, *On a procedure to derive ϵ-factorised differential equations beyond polylogarithms*, *JHEP* **07** (2023) 206 [arXiv:2305.14090] [INSPIRE].

[85] F. Moriello, *Generalised power series expansions for the elliptic planar families of Higgs + jet production at two loops*, *JHEP* **01** (2020) 150 [arXiv:1907.13234] [INSPIRE].

[86] F.V. Tkachov, *A theorem on analytical calculability of 4-loop renormalization group functions*, *Phys. Lett. B* **100** (1981) 65 [INSPIRE].

[87] K.G. Chetyrkin and F.V. Tkachov, *Integration by parts: The algorithm to calculate β-functions in 4 loops*, *Nucl. Phys. B* **192** (1981) 159 [INSPIRE].

[88] R.N. Lee, *Presenting LiteRed: a tool for the Loop InTEgrals REDuction*, arXiv:1212.2685 [INSPIRE].

[89] R.N. Lee, *LiteRed 1.4: a powerful tool for reduction of multiloop integrals*, *J. Phys. Conf. Ser.* **523** (2014) 012059 [arXiv:1310.1145] [INSPIRE].

[90] Z. Wu et al., *NeatIBP 1.0, a package generating small-size integration-by-parts relations for Feynman integrals*, *Comput. Phys. Commun.* **295** (2024) 108999 [arXiv:2305.08783] [INSPIRE].

[91] J. Gluza, K. Kajda and D.A. Kosower, *Towards a Basis for Planar Two-Loop Integrals*, *Phys. Rev. D* **83** (2011) 045012 [arXiv:1009.0472] [INSPIRE].

[92] S. Laporta, *High-precision calculation of multiloop Feynman integrals by difference equations*, *Int. J. Mod. Phys. A* **15** (2000) 5087 [hep-ph/0102033] [INSPIRE].

[93] T. Peraro, *Analytic multi-loop results using finite fields and dataflow graphs with FiniteFlow*, in the proceedings of the *14th International Symposium on Radiative Corrections: Application of Quantum Field Theory to Phenomenology*, Avignon, France, September 08–13 (2019) [DOI:10.22323/1.375.0077] [arXiv:1912.03142] [INSPIRE].

[94] S. Pozzorini and E. Remiddi, *Precise numerical evaluation of the two loop sunrise graph master integrals in the equal mass case*, *Comput. Phys. Commun.* **175** (2006) 381 [hep-ph/0505041] [INSPIRE].

[95] U. Aglietti, R. Bonciani, L. Grassi and E. Remiddi, *The two loop crossed ladder vertex diagram with two massive exchanges*, *Nucl. Phys. B* **789** (2008) 45 [arXiv:0705.2616] [INSPIRE].

[96] R.N. Lee, A.V. Smirnov and V.A. Smirnov, *Solving differential equations for Feynman integrals by expansions near singular points*, *JHEP* **03** (2018) 008 [arXiv:1709.07525] [INSPIRE].

[97] R.N. Lee, A.V. Smirnov and V.A. Smirnov, *Evaluating 'elliptic' master integrals at special kinematic values: using differential equations and their solutions via expansions near singular points*, *JHEP* **07** (2018) 102 [arXiv:1805.00227] [INSPIRE].

[98] R. Bonciani, G. Degrassi, P.P. Giardino and R. Gröber, *A Numerical Routine for the Crossed Vertex Diagram with a Massive-Particle Loop*, *Comput. Phys. Commun.* **241** (2019) 122 [arXiv:1812.02698] [INSPIRE].

[99] M. Fael, F. Lange, K. Schönwald and M. Steinhauser, *A semi-analytic method to compute Feynman integrals applied to four-loop corrections to the $\overline{\text{MS}}$-pole quark mass relation*, *JHEP* **09** (2021) 152 [arXiv:2106.05296] [INSPIRE].

[100] M. Fael, F. Lange, K. Schönwald and M. Steinhauser, *Massive Vector Form Factors to Three Loops*, *Phys. Rev. Lett.* **128** (2022) 172003 [arXiv:2202.05276] [INSPIRE].

JHEP07(2024)073

[101] M. Hidding, *DiffExp, a Mathematica package for computing Feynman integrals in terms of one-dimensional series expansions*, *Comput. Phys. Commun.* **269** (2021) 108125 [arXiv:2006.05510] [INSPIRE].

[102] X. Liu and Y.-Q. Ma, *AMFlow: A mathematica package for Feynman integrals computation via auxiliary mass flow*, *Comput. Phys. Commun.* **283** (2023) 108565 [arXiv:2201.11669] [INSPIRE].

[103] T. Armadillo et al., *Evaluation of Feynman integrals with arbitrary complex masses via series expansions*, *Comput. Phys. Commun.* **282** (2023) 108545 [arXiv:2205.03345] [INSPIRE].

[104] X. Liu, Y.-Q. Ma and C.-Y. Wang, *A Systematic and Efficient Method to Compute Multi-loop Master Integrals*, *Phys. Lett. B* **779** (2018) 353 [arXiv:1711.09572] [INSPIRE].

[105] X. Liu and Y.-Q. Ma, *Multiloop corrections for collider processes using auxiliary mass flow*, *Phys. Rev. D* **105** (2022) L051503 [arXiv:2107.01864] [INSPIRE].

[106] Z.-F. Liu and Y.-Q. Ma, *Automatic computation of Feynman integrals containing linear propagators via auxiliary mass flow*, *Phys. Rev. D* **105** (2022) 074003 [arXiv:2201.11636] [INSPIRE].

[107] N. Arkani-Hamed et al., *The All-Loop Integrand For Scattering Amplitudes in Planar $N = 4$ SYM*, *JHEP* **01** (2011) 041 [arXiv:1008.2958] [INSPIRE].

[108] N. Arkani-Hamed, J.L. Bourjaily, F. Cachazo and J. Trnka, *Local Integrals for Planar Scattering Amplitudes*, *JHEP* **06** (2012) 125 [arXiv:1012.6032] [INSPIRE].

[109] S. Badger, G. Mogull and T. Peraro, *Local integrands for two-loop all-plus Yang-Mills amplitudes*, *JHEP* **08** (2016) 063 [arXiv:1606.02244] [INSPIRE].

[110] G. Barucchi and G. Ponzano, *Differential equations for one-loop generalized feynman integrals*, *J. Math. Phys.* **14** (1973) 396 [INSPIRE].

[111] A.V. Kotikov, *Differential equations method: The calculation of vertex type Feynman diagrams*, *Phys. Lett. B* **259** (1991) 314 [INSPIRE].

[112] T. Gehrmann and E. Remiddi, *Differential equations for two loop four point functions*, *Nucl. Phys. B* **580** (2000) 485 [hep-ph/9912329] [INSPIRE].

[113] Z. Bern, L.J. Dixon and D.A. Kosower, *Dimensionally regulated pentagon integrals*, *Nucl. Phys. B* **412** (1994) 751 [hep-ph/9306240] [INSPIRE].

[114] K.-T. Chen, *Iterated path integrals*, *Bull. Am. Math. Soc.* **83** (1977) 831 [INSPIRE].

[115] A.B. Goncharov, M. Spradlin, C. Vergu and A. Volovich, *Classical Polylogarithms for Amplitudes and Wilson Loops*, *Phys. Rev. Lett.* **105** (2010) 151605 [arXiv:1006.5703] [INSPIRE].

[116] S. Badger, J. Kryś, R. Moodie and S. Zoia, *Lepton-pair scattering with an off-shell and an on-shell photon at two loops in massless QED*, *JHEP* **11** (2023) 041 [arXiv:2307.03098] [INSPIRE].

[117] A. Primo and L. Tancredi, *On the maximal cut of Feynman integrals and the solution of their differential equations*, *Nucl. Phys. B* **916** (2017) 94 [arXiv:1610.08397] [INSPIRE].

[118] T. Gehrmann, A. von Manteuffel, L. Tancredi and E. Weihs, *The two-loop master integrals for $q\bar{q} \to VV$*, *JHEP* **06** (2014) 032 [arXiv:1404.4853] [INSPIRE].

[119] S. Müller-Stach, S. Weinzierl and R. Zayadeh, *Picard-Fuchs equations for Feynman integrals*, *Commun. Math. Phys.* **326** (2014) 237 [arXiv:1212.4389] [INSPIRE].

JHEP07(2024)073

[120] L. Adams, E. Chaubey and S. Weinzierl, *Simplifying Differential Equations for Multiscale Feynman Integrals beyond Multiple Polylogarithms*, *Phys. Rev. Lett.* **118** (2017) 141602 [arXiv:1702.04279] [INSPIRE].

[121] H. Frellesvig, *On epsilon factorized differential equations for elliptic Feynman integrals*, *JHEP* **03** (2022) 079 [arXiv:2110.07968] [INSPIRE].

[122] O.V. Tarasov, *Connection between Feynman integrals having different values of the space-time dimension*, *Phys. Rev. D* **54** (1996) 6479 [hep-th/9606018] [INSPIRE].

[123] S. Badger, M. Becchetti, N. Giraudo and S. Zoia, *Ancillary files for "Two-loop integrals for $t\bar{t}$+jet production at hadron colliders in the leading colour approximation"*, (2024), https://zenodo.org/records/10935012.

[124] M. van Hoeij, *Factorization of differential operators with rational functions coefficients*, *J. Symb. Comput.* **24** (1997) 537.

[125] S. Weinzierl, *Feynman Integrals*, arXiv:2201.03593 [DOI:10.1007/978-3-030-99558-4] [INSPIRE].

[126] A. Hodges, *Eliminating spurious poles from gauge-theoretic amplitudes*, *JHEP* **05** (2013) 135 [arXiv:0905.1473] [INSPIRE].

[127] S. Zoia, *Modern Analytic Methods for Computing Scattering Amplitudes: With Application to Two-Loop Five-Particle Processes*, (2022), DOI:10.1007/978-3-031-01945-6 [INSPIRE].

[128] M. Heller, A. von Manteuffel and R.M. Schabinger, *Multiple polylogarithms with algebraic arguments and the two-loop EW-QCD Drell-Yan master integrals*, *Phys. Rev. D* **102** (2020) 016025 [arXiv:1907.00491] [INSPIRE].

[129] X. Jiang, J. Liu, X. Xu and L.L. Yang, *Symbol letters of Feynman integrals from Gram determinants*, arXiv:2401.07632 [INSPIRE].

[130] S. Caron-Huot and J.M. Henn, *Iterative structure of finite loop integrals*, *JHEP* **06** (2014) 114 [arXiv:1404.2922] [INSPIRE].

[131] D. Gaiotto, J. Maldacena, A. Sever and P. Vieira, *Pulling the straps of polygons*, *JHEP* **12** (2011) 011 [arXiv:1102.0062] [INSPIRE].

[132] H.R.P. Ferguson and D.H. Bailey, *A Polynomial Time, Numerically Stable Integer Relation Algorithm*, *RNR Technical Report RNR-91-032* (1992).

[133] M. Becchetti et al., *Next-to-leading order corrections to light-quark mixed QCD-EW contributions to Higgs boson production*, *Phys. Rev. D* **103** (2021) 054037 [arXiv:2010.09451] [INSPIRE].

[134] R. Bonciani et al., *Next-to-leading-order QCD corrections to Higgs production in association with a jet*, *Phys. Lett. B* **843** (2023) 137995 [arXiv:2206.10490] [INSPIRE].

[135] T. Armadillo et al., *Two-loop mixed QCD-EW corrections to neutral current Drell-Yan*, *JHEP* **05** (2022) 072 [arXiv:2201.01754] [INSPIRE].

[136] R. Bonciani et al., *Mixed Strong-Electroweak Corrections to the Drell-Yan Process*, *Phys. Rev. Lett.* **128** (2022) 012002 [arXiv:2106.11953] [INSPIRE].

[137] M. Becchetti et al., *Full top-quark mass dependence in diphoton production at NNLO in QCD*, *Phys. Lett. B* **848** (2024) 138362 [arXiv:2308.10885] [INSPIRE].

[138] P.A. Baikov, *Explicit solutions of the multiloop integral recurrence relations and its application*, *Nucl. Instrum. Meth. A* **389** (1997) 347 [hep-ph/9611449] [INSPIRE].

[139] H. Frellesvig and C.G. Papadopoulos, *Cuts of Feynman Integrals in Baikov representation*, *JHEP* **04** (2017) 083 [arXiv:1701.07356] [INSPIRE].

JHEP07(2024)073